

# **Shared Decision-Making and Control Between Humans and Adaptive Control Algorithms**

by

Benjamin T. Thomsen

B.Eng., McGill University (2015)

Submitted to the Department of Mechanical Engineering  
in partial fulfillment of the requirements for the degree of  
Master of Science in Mechanical Engineering

at the

MASSACHUSETTS INSTITUTE OF TECHNOLOGY

June 2018

© Massachusetts Institute of Technology 2018. All rights reserved.

Author .....  
Department of Mechanical Engineering  
May 23, 2018

Certified by .....  
Anuradha M. Annaswamy  
Senior Research Scientist  
Thesis Supervisor

Accepted by .....  
Rohan Abeyaratne  
Chairman, Department Committee on Graduate Theses



# **Shared Decision-Making and Control Between Humans and Adaptive Control Algorithms**

by

Benjamin T. Thomsen

Submitted to the Department of Mechanical Engineering  
on May 23, 2018, in partial fulfillment of the  
requirements for the degree of  
Master of Science in Mechanical Engineering

## **Abstract**

This thesis addresses the problem of controlling a dynamical system subject to both parametric uncertainties and abrupt changes in the dynamic structure of the system, by proposing a shared control architecture predicated on a suitable division of responsibilities between supervisory human operators and adaptive control algorithms. Dynamical anomalies, such as the sudden introduction of unmodeled dynamics or time delays, present difficulties in control for both human operators and autonomous model-based control algorithms. Online adjustment to extenuate the effects of parametric uncertainty is possible through the proper use of adaptive control, and to a certain extent is paralleled by the learning of dynamics and adaptation of control policies by humans. Changes to the dynamic structure of the system, however, may lead to poor closed-loop performance and instability, regardless of whether the control input is determined by a human or adaptive control algorithm.

The shared decision-making and control architecture introduced in this thesis tasks supervisory human operators with several high-level responsibilities in the mitigation of dynamical anomalies, and utilizes adaptive control algorithms for low-level control and command tracking duties. The shared controller is defined for dynamical systems where the full state is assumed to be measured as well as the case where only certain outputs are measured. The ability to respond to anomalies using this shared control architecture is demonstrated in several simulations of scenarios related to flight control, including the longitudinal control of an unmanned aerial vehicle whose actuator dynamics abruptly change from first-order to second-order, and the lateral-directional control of a fixed-wing aircraft subject to two anomalies concerning actuator dynamics and sensor dynamics. These simulations demonstrate how the division of responsibilities proposed in this thesis enables the recovery of closed-loop system stability and command tracking performance following the aforementioned anomalies.

Thesis Supervisor: Anuradha M. Annaswamy  
Title: Senior Research Scientist



## Acknowledgments

I would like to thank my advisor, Dr. Anuradha Annaswamy for providing the instruction and support I needed to succeed in my research endeavors, and for teaching me how to approach unfamiliar subjects. I appreciate all the time she has devoted to clearing the hurdles for this work to progress, and to helping me learn to research effectively. I would like to thank Dr. Eugene Lavretsky for his enthusiastic support of my research, and for his valuable perspectives which have inspired me to think about the practical aspects of control design.

I owe thanks to all my colleagues in the Active Adaptive Control Laboratory for their guidance, teaching, and support which has contributed to this research. I would like to thank Max Zheng Qu in particular, whose advancements in adaptive control theory proved to be very useful in the development of this work, and whose repositories of code for control design and aircraft modeling and simulation saved me countless hours. Heather Hussain, Joey Gaudio, and Bitzy Flamholz have been invaluable resources to discuss ideas with, and I am grateful for the time they set aside to help me explore research ideas.

I am thankful for the support and inspiration of my friends throughout my time at MIT. Finally, I owe a great deal of gratitude to my parents for inspiring my passion for science and engineering that led me here.

THIS PAGE INTENTIONALLY LEFT BLANK

# Contents

<b>1</b>	<b>Introduction</b>	<b>15</b>
1.1	Background . . . . .	15
1.2	Contributions . . . . .	19
<b>2</b>	<b>Problem Statement</b>	<b>21</b>
2.1	Aircraft with On-Board Human Pilot and Full State Measurements . .	21
2.1.1	Actuator Fault . . . . .	23
2.1.2	Time-Delayed Sensor Measurements . . . . .	24
2.2	Aircraft with Remote Human Pilot and Output Measurements . . . .	25
2.2.1	Actuator Fault . . . . .	25
<b>3</b>	<b>Shared Control with Human Pilot and State Feedback</b>	<b>29</b>
3.1	Full-State Feedback Adaptive Autopilot . . . . .	29
3.1.1	Nominal Adaptive Controller . . . . .	30
3.1.2	Recovery Adaptive Controller . . . . .	33
3.2	Human Pilot . . . . .	34
3.3	Overall Shared Controller . . . . .	35
<b>4</b>	<b>Shared Control with Remote Human Pilot and Output Feedback</b>	<b>39</b>
4.1	Output Feedback Adaptive Autopilot . . . . .	40
4.1.1	Nominal Adaptive Controller . . . . .	42
4.1.2	Recovery Adaptive Controller . . . . .	44
4.2	Remote Human Pilot . . . . .	48

4.3	Overall Shared Controller . . . . .	48
<b>5</b>	<b>Simulated Anomaly Response Scenarios</b>	<b>51</b>
5.1	SISO State Feedback and On-Board Pilot . . . . .	51
5.1.1	Aircraft Rolling Mode Dynamics . . . . .	51
5.1.2	Actuator Fault Simulations . . . . .	55
5.1.3	Sensor Latency Simulations . . . . .	58
5.2	MIMO Output Feedback and Remote Pilot . . . . .	64
5.2.1	HALE Aircraft Longitudinal Dynamics . . . . .	64
5.2.2	Simulations . . . . .	68
<b>6</b>	<b>Concluding Remarks</b>	<b>79</b>
<b>A</b>	<b>Numerical Simulation Parameters</b>	<b>81</b>

# List of Figures

1-1	General architecture for shared decision-making and control of complex dynamical systems, adapted from Ref. [33]. Signals labeled $r$ , $u$ , $x$ , and $y$ represent commands, control input, plant state, and measured plant output, respectively. The signals $y_D$ and $y_H$ represent plant output information available to the human supervisor via display interfaces and through the human's internal sensory modalities (such as the proprioceptive and vestibular systems), respectively. . . . .	18
2-1	Supervisory operation of a fleet of high altitude, long endurance UAVs by remote human operator . . . . .	26
3-1	Block diagram of model reference adaptive controller with closed-loop reference model and full-state feedback . . . . .	32
3-2	Proposed framework for shared decision-making and control between an on-board human pilot and adaptive control algorithms following an anomaly, with roles organized by stages of decision making as categorized in Ref. [26] . . . . .	36
4-1	Proposed framework for shared decision-making and control between a remote human operator and adaptive control algorithms following an anomaly, with roles organized by stages of decision making as categorized in Ref. [26] . . . . .	49

5-1	Act-AR simulation: Bank angle command ( $r(t)$ ) and output ( $\phi(t)$ ) in nominal operation ( $t \leq t_1^*$ ), after change in actuator dynamics ( $t_1^* < t \leq t_2^*$ ), and after a corrective action ( $t > t_2^*$ ) . . . . .	56
5-2	Act-AR simulation: Adaptive feedback gains in nominal operation ( $t \leq t_1^*$ ), after change in actuator dynamics ( $t_1^* < t \leq t_2^*$ ), and after a corrective action ( $t > t_2^*$ ) . . . . .	57
5-3	Act-AR simulation: Tracking error $\ e(t)\ $ in nominal operation ( $t \leq t_1^*$ ), after change in actuator dynamics ( $t_1^* < t \leq t_2^*$ ), and after a corrective action ( $t > t_2^*$ ) . . . . .	57
5-4	Act-AR analysis: Unit step responses for closed-loop transfer functions at different stages of simulation, demonstrating performance improvement after corrective action . . . . .	58
5-5	Del-AR simulation: Bank angle command ( $r(t)$ ) and output ( $\phi(t)$ ) in nominal operation ( $t \leq t_1^*$ ), after abrupt addition of a time delay ( $t_1^* < t \leq t_2^*$ ), and after a corrective action ( $t > t_2^*$ ) . . . . .	60
5-6	Del-AR simulation: Adaptive feedback gains in nominal operation ( $t \leq t_1^*$ ), after abrupt addition of a time delay ( $t_1^* < t \leq t_2^*$ ), and after a corrective action ( $t > t_2^*$ ) . . . . .	61
5-7	Del-AR simulation: Tracking error $\ e(t)\ $ in nominal operation ( $t \leq t_1^*$ ), after abrupt addition of a time delay ( $t_1^* < t \leq t_2^*$ ), and after a corrective action ( $t > t_2^*$ ) . . . . .	61
5-8	Del-AR analysis: Unit step responses for closed-loop transfer functions at different stages of simulation, demonstrating performance improvement after corrective action . . . . .	62
5-9	Del-AR-P simulation (passive anomaly response): The vehicle loses closed-loop stability following the anomaly when the shared control response is not implemented, and failure occurs at $t = t_3^*$ . . . . .	63
5-10	Rendering of very flexible aircraft model used in numerical simulations	64
5-11	Poles of linearized open-loop HALE VFA dynamics for different dihedral angles, in the complex plane . . . . .	67

5-12 Dominant poles of linearized open-loop HALE VFA dynamics, which move into the right-half complex plane when $\eta > 11^\circ$ . . . . .	67
5-13 Actuator trim at different dihedral angles . . . . .	67
5-14 Nom-1 simulation: Control of longitudinal dynamics of VFA model using RSLQR, with no uncertainty in the control model . . . . .	69
5-15 Nom-2 simulation: Control of longitudinal dynamics of VFA model using RSLQR, with uncertainties $\Theta_p$ , $\Lambda_p$ , and $\Theta_1$ . . . . .	70
5-16 Nom-3 simulation: Control of longitudinal dynamics of VFA model using RSLQR + adaptive control, with uncertainties $\Theta_p$ , $\Lambda_p$ , and $\Theta_1$ .	71
5-17 AR-1 simulation: Passive response to dynamical anomaly results in structural failure after 6 minutes . . . . .	73
5-18 AR-1 simulation: Adaptive parameters diverge as controller struggles to adapt to unmodeled dynamics . . . . .	74
5-19 AR-1 simulation: Model-following output error and command tracking error grow due to anomalous dynamics . . . . .	74
5-20 AR-1-LQR simulation: Passive response to dynamical anomaly using only baseline RSLQR control (no adaptive) also results in structural failure . . . . .	75
5-21 AR-3 simulation: Shared response to the dynamical anomaly results in recovery of vehicle performance . . . . .	76
5-22 AR-3 simulation: The change in control model at $t_2^* = 800s$ stops the divergence of adaptive parameters . . . . .	77
5-23 AR-3 simulation: The change in control model at $t_2^* = 800s$ stops the error growth seen after the anomaly . . . . .	77

THIS PAGE INTENTIONALLY LEFT BLANK

# List of Tables

5.1	Summary of the simulations presented in Chapter 5. $t_1^*$ denotes the time of anomaly occurrence, $t_2^*$ denotes the time of the human completing anomaly response tasks, $t_3^*$ denotes the time of plant/controller failure, $t_{\text{sim}}$ denotes the simulation length. . . . .	78
A.1	Parameters used in the <i>nominal</i> adaptive controller for numerical HALE VFA simulations . . . . .	81
A.2	Parameters used in the <i>recovery</i> adaptive controller for numerical HALE VFA simulations . . . . .	82

THIS PAGE INTENTIONALLY LEFT BLANK

# Chapter 1

## Introduction

### 1.1 Background

Model-based feedback control techniques, which can establish measures of stability, optimality, and closed-loop dynamic characteristics explicitly in control design, are predicated on a certain level of *a priori* knowledge of system dynamics. In any complex dynamical system, however, uncertainty is inevitable. Uncertainty may be present for myriad reasons including modeling errors, environmental variations, unforeseen anomalies, and external disturbances. The field of adaptive control addresses a limitation of control based on models of system dynamics, namely that parameters used to model the system may be uncertain. Adaptive control [24, 20] accommodates these parametric uncertainties through online tuning of control parameters to ensure specified closed-loop dynamics are realized. Recent advances in adaptive control have included the development of closed-loop reference models (CRMs) [8], which greatly improves transient performance during online learning. Guarantees of stability and tracking convergence are obtained under a few assumptions on the underlying modeling structure. One such assumption includes knowledge of the order of the system dynamics for control design. This in turn is used to determine the number of adjustable parameters which in turn represent the key adaptive elements of an adaptive controller.

Human operators of dynamical systems also develop mental models of expected

dynamic behavior, often over long periods of active learning. Humans have been modeled and studied extensively in the domains of flight control [13, 39, 23, 27] and driving [21] to examine their use of information feedback and ability to adapt their control strategies to unfamiliar situations. Human pilots, for example, are found to have limits when attempting to rapidly learn unfamiliar and anomalous vehicle dynamics [12, 13, 4, 39, 25]. In stressful situations, human pilots tend to apply high control gains, which coupled with certain dynamical anomalies may lead to pilot-induced oscillations and an increased risk of loss of control [10]. Recent research has investigated pilot adaptation to time-varying dynamics [11, 13, 40]. In Ref. [39], the author used maximum-likelihood estimation techniques to model pilot adaptation to sudden and unexpected changes in dynamics in a flight simulation environment, and control performance was shown to degrade after a change in vehicle dynamics to something unfamiliar, even as the pilots adapted their feedback strategies to try to recover performance. A recent study found that the majority of transport aircraft loss of control incidents over a 15-year period involved inaction or improper action by the flight crew [2]. Endsley (1996) points to pilot error following a transition from autonomous to manual control (often as the result of an anomaly) as a common factor in loss of control incidents [5].

Issues with manual control of dynamical systems are exacerbated when the human operator is physically separated from the dynamics of the system, as is the case with remotely piloted vehicles [22, 37]. The additional complexities involved with remote operation include a lack of sensory and perceptive cues regarding the vehicle (or the *plant*, in general) state and its environment, time delays between the dynamical system and operator for both sensing and actuation, and difficulty ascertaining the open-loop dynamical response between control input and plant output [17, 18]. Tvaryanas and Thompson found that over a 10-year period, more than 50% of mishaps with US Air Force MQ-1 Predator remotely piloted aircraft were caused by active failures by human operators and crewmembers [37].

This naturally leads one to address the problem of how the limitations of autonomous control systems based on adaptive control algorithms (as in Refs. [24] and

[20]) and those of the human operators can be overcome by sharing decision-making and control tasks between adaptive control algorithms and human operators. The goal of this work is to develop one such framework where a supervisory human operator takes a targeted and active role in response to anomalous system behavior, allowing an adaptive control algorithm to suitably adapt to the abrupt introduction of anomalous dynamics and recover closed-loop control performance.

Anomalies in aircraft dynamical behavior can come from a number of sources, such as sensor or actuator system failures or malfunctions, changes to the inertial properties of the aircraft, structural damage, and foreign object damage [3]. As aerial vehicles increasingly depend on networked systems for guidance and navigation, there is a need to consider not only physical failures but also anomalies which may affect data signals, such as cyber attacks. Advanced aircraft navigation systems, which rely on the fusion of various digital sources of information to estimate the vehicle state and to guide and control the vehicle present new vulnerabilities which can have severe consequences in safety and control performance [15, 14, 16, 1]. The response to an anomaly in semi-autonomous flight is generally to transfer control to the human pilot unless the aircraft is equipped with active fault-tolerant control systems (AFTCS) that have been designed to handle the particular type of anomaly [41]. The latter requires fault detection and diagnosis schemes which are able to correctly and consistently detect, isolate, and diagnose anomalous and unfamiliar behavior. State of the art AFTCS which use model-based fault detection and diagnosis are only able to retain autonomous control after anomalies which are well-defined and likely to be properly diagnosed, and for which a reconfigurable controller has been extensively verified and validated [41].

To maximize the probability of detection of an anomaly while minimizing the probability of false alarm, it may be advantageous to include the human operator in tasks relating to the detection and diagnosis of dynamical anomalies [34]. In particular, given that the anomaly response consists broadly of (a) perception of the anomaly, and (b) mitigation of the anomaly effects through suitable correction and compensation, the question is whether a human operator can perform step (a) and

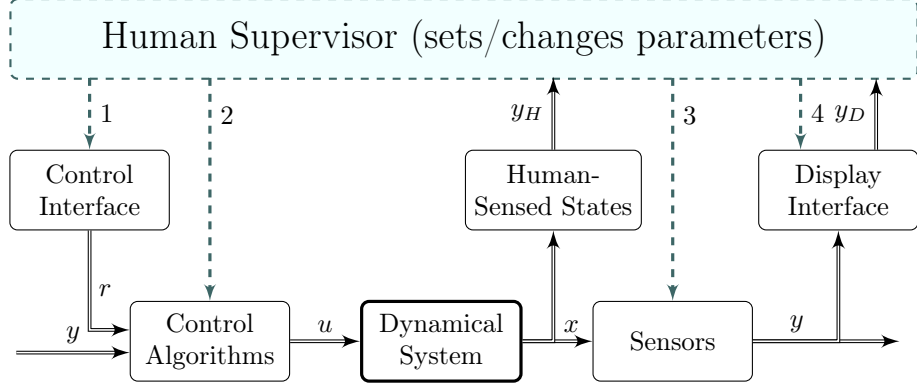


Figure 1-1: General architecture for shared decision-making and control of complex dynamical systems, adapted from Ref. [33]. Signals labeled  $r$ ,  $u$ ,  $x$ , and  $y$  represent commands, control input, plant state, and measured plant output, respectively. The signals  $y_D$  and  $y_H$  represent plant output information available to the human supervisor via display interfaces and through the human’s internal sensory modalities (such as the proprioceptive and vestibular systems), respectively.

adaptive control algorithms can be used to perform step (b). This task allocation can be thought of as a type of supervisory control [32, 33]. Figure 1-1 shows a supervisory control structure based on that of Ref. [33], where the human supervisor has several pathways through which to interact with the plant and controller. The human supervisor is able to perceive via pathway  $y_H$  (sensing via sensory modalities internal to the human) and via pathway  $y_D$  (information from the plant’s sensors displayed to the human through an interface). The human supervisor is able to provide input through the pathways 1–4, which may affect the signals  $r$ ,  $u$ ,  $y$ , and  $y_D$ , respectively. A division of responsibilities similar to that proposed in this thesis has been investigated recently in Ref. [6], where the pilot’s role is to provide an initial estimate of the anomaly severity, which is then used by an adaptive autopilot to determine a reference model and estimates of control parameters. Unlike Ref. [6], more complex anomalies which are assumed to significantly alter the plant model structure are considered in this thesis, and synergetic architectures are explored to leverage the merits of both the human operator and adaptive control algorithms in an effective response to anomalies.

## 1.2 Contributions

This thesis develops and demonstrates a shared decision-making and control architecture between humans and adaptive control algorithms. This architecture is considered in the context of flight control, where system architectures often include both supervisory human operators and autonomous flight control systems. This shared control architecture is based on the use of adaptive control algorithms to manage uncertainty in dynamics, and supervisory human operators who manage a shared response to anomalous changes in the structure of plant dynamics. This thesis will demonstrate and discuss how this shared decision-making and control architecture enables overall adaptive capabilities beyond what humans or adaptive control algorithms alone could accomplish, by making use of the benefits of collaboration between humans and adaptive control algorithms.

This thesis is organized as follows. Chapter 2 states the problem of control of a plant in the presence of parametric uncertainties as well as sudden dynamical anomalies, which are defined in more detail. Chapter 3 presents the shared decision-making and control architecture in a simplified example, using control algorithms with a scalar input and access to the full plant state, and with a human pilot present on-board. Chapter 4 extends this shared decision-making and control architecture to a multi-input multi-output plant model with control design based on output feedback and remote human operators. In Chapter 5, it is shown that the resulting shared controllers perform satisfactorily through extensive numerical simulation studies. Concluding remarks are given in Chapter 6.

THIS PAGE INTENTIONALLY LEFT BLANK

# Chapter 2

## Problem Statement

This thesis considers two control problems, which will be described in Sections 2.1 and 2.2, and addressed in Chapters 3 and 4, respectively. In the first problem, it is assumed that the plant has a single input and single output, and that the full state of the plant is measured directly. In this problem it is also assumed that the plant is an aircraft which has a pilot on-board. In the second problem, the plant is assumed to have multiple inputs and multiple outputs, while only the plant outputs are measured. In this second problem, the plant is assumed to be an unmanned aircraft with a remote human operator. This thesis posits that both of these problems may be addressed by designing shared control architectures which make use of collaboration between humans and adaptive control algorithms.

### 2.1 Aircraft with On-Board Human Pilot and Full State Measurements

We consider single-input single-output (SISO)  $n$ th-order linear dynamical plant models of the form

$$\dot{x}_p = A_p x_p + B_p u_p, \quad y_p = C_p x_p \quad (2.1)$$

where  $x_p(t) \in \mathbb{R}^{n \times 1}$  is the state vector,  $A_p \in \mathbb{R}^{n \times n}$  and  $B_p \in \mathbb{R}^{n \times 1}$  are an uncertain matrix and an uncertain vector of dynamical properties, respectively, and  $u_p(t)$  is a

scalar input.  $C_p \in \mathbb{R}^{1 \times n}$  is a known vector producing the scalar plant output,  $y_p(t)$ , which we would like to follow prescribed commands  $r(t)$  by providing a control action  $u(t)$ . For this problem, we consider the case where the vector  $x_p$ , consisting of the output  $y_p$  and its first  $n - 1$  time derivatives, is measured and available for use in feedback control, and the vector  $B_p$  is given by  $B_p = [0, \dots, 0, \beta]^T$ . We note that plants of this form have a transfer function from plant input to output given in the Laplace frequency domain by

$$\frac{Y_p(s)}{U_p(s)} = \frac{\beta}{s^n + \alpha_{n-1}s^{n-1} + \dots + \alpha_0} \quad (2.2)$$

where  $\alpha_i$  and  $\beta$  are arbitrary coefficients. Design of the control law  $u(t)$  is carried out under nominal conditions with the assumption

$$u_p(t) \equiv u(t). \quad (2.3)$$

Note that uncertainty in control effectiveness is captured by the uncertain matrix  $B_p$ .

In addition to an autonomous controller which generates control input  $u(t)$  in (2.3), a human operator (pilot) is tasked with the high-level operation of the plant (2.1), including monitoring to ensure safe and anomaly-free operation. Operation is denoted *human-on-the-loop* as opposed to *human-in-the-loop*, as the pilot does not directly command actuator input. The pilot's perceptive capabilities (corresponding to the pathways in Figure 1-1) are assumed to include the sensing of  $y_D \subseteq y$ ,  $y_H$ , and  $r$ , where  $y_D$  is a subset of vehicle sensor measurements available to the pilot through cockpit displays,  $y_H$  is the human pilot's sensing through visual and vestibular modalities, and  $r$  is the prescribed command which the plant output should track. Note that in the single output case,  $y_D \equiv y$ .

We consider the introduction of two severe anomalies in the dynamics of the plant model (2.1), described in Sections 2.1.1 and 2.1.2. The first consists of a change in the actuator dynamics, represented as a change in the actuator model from a gain to a first-order lag. The second anomaly is a latency introduced in the feedback of state information to the control algorithms.

The problem we investigate in Chapter 3 is whether the design of  $u(t)$  can be carried out using a shared decision-making and control architecture which leverages the merits of

- (a) autonomous control methodologies
- (b) an on-board human pilot

to successfully mitigate two types of anomalous dynamics to be described presently and restore tracking performance in the presence of uncertainty. We refer to this class of anomaly response as a shared control response. The following two subsections describe two specific anomalies which will be addressed using this shared controller in Chapter 3.

### 2.1.1 Actuator Fault

An anomaly is introduced which changes the actuator dynamics from a direct input (2.3) to a first-order lag

$$T_L \dot{u}(t) + u(t) = u_p(t) \quad (2.4)$$

so that the dynamics of plant augmented with actuator dynamics change suddenly from order  $n$  to order  $n + 1$ . We can define an augmented plant

$$\dot{x}'_p = A'_p x'_p + B'_p u \quad (2.5)$$

where  $u(t)$  is defined in (2.4), and  $x'_p(t)$  consists of the output  $y_p(t)$  and its first  $n$  time derivatives. The matrix  $A'_p$  and vector  $B'_p$  are then given by

$$A'_p = \begin{bmatrix} 0 & \begin{bmatrix} I_n \end{bmatrix} \\ \vdots & \\ \alpha'_0 & \cdots & \alpha'_{n+1} \end{bmatrix}, \quad B'_p = \begin{bmatrix} 0 \\ \vdots \\ \beta' \end{bmatrix} \quad (2.6)$$

where  $I_n$  is the identity matrix of dimension  $n$  and  $\alpha'_i, \beta'$  are uncertain coefficients. If the change in the order of the plant is not known to the adaptive controller, it

may no longer be possible for it to stabilize the plant following such a change. The question then is if a shared decision-making architecture, with suitable action from the human pilot leading to feedback on the augmented state vector  $x'_p$ , can result in the recovery of closed-loop performance with anomalous actuator model (2.4) and parametric uncertainties in the plant (2.5).

### 2.1.2 Time-Delayed Sensor Measurements

We consider the introduction of an anomaly which leads to latency in the measurement of plant state information. We model this anomaly as the addition of a time delay  $\tau$  of the state measurements before the computation of the control input, causing a discrepancy between the current plant state  $x_p(t)$  and the state as sensed by the controller, denoted  $x_\sigma(t)$ , given by

$$x_\sigma(t) = x_p(t - \tau). \quad (2.7)$$

We note that the effect of the time delay  $\tau$  may be approximated as a first-order filter, given in the Laplace frequency domain as

$$e^{-\tau s} \approx \frac{1}{1 + \tau s}. \quad (2.8)$$

In the time domain, this approximation corresponds to the differential equation

$$\tau \dot{x}_\sigma(t) + x_\sigma(t) \approx x_p(t) \quad (2.9)$$

We note that this effectively increases the order of the plant from  $n$  to  $n + 1$  when we consider the output to be the delayed signal. In this case, using the time delay approximation of (2.9), the augmented plant model is given by

$$\dot{x}'_\sigma = A'_p x'_\sigma + B'_p u \quad (2.10)$$

with  $A'_p$  and  $B'_p$  defined in (2.6). Due to this similarity, we investigate the applicability

of a shared control solution to the problem of Section 2.1.1 to the problem of a time-delayed state measurement. The shared control architecture which we propose to address these two problems is presented in Chapter 3.

## 2.2 Aircraft with Remote Human Pilot and Output Measurements

Here we consider the problem of controlling linear multi-input multi-output (MIMO) plant models of the form

$$\begin{aligned}\dot{x}_p &= (A_p + B_p \Theta_p^T)x_p + B_p \Lambda_p u_p \\ y_p &= C_p x_p, \quad z_p = C_{pz} x_p\end{aligned}\tag{2.11}$$

where  $x_p$  is the plant state,  $u_p$  is the plant input,  $y_p$  is measured output, and  $z_p$  is regulated output. Uncertain dynamics lead to the introduction of unknown  $\Theta_p$  and  $\Lambda_p$  in the plant model. It is assumed that the matrix  $CB$  has full rank, and thus the plant has uniform relative degree one (see [31]). In addition to the dynamics (2.11), the plant's actuators have the first-order dynamics

$$\dot{u}_p + (D_1 + \Theta_1^T)u_p = D_1 u \tag{2.12}$$

where  $D_1$  is a diagonal matrix representing nominal actuator parameters and  $\Theta_1$  models uncertainty in the actuator dynamics. The problem is to choose  $u(t)$  such that  $z_p(t)$  tracks an external command  $z_{cmd}(t)$  as closely as possible.

### 2.2.1 Actuator Fault

Consider the occurrence of an anomaly which causes an abrupt change in actuator dynamics from (2.12) to the second-order model

$$\ddot{u}_p + (D_2 + \Theta_2^T)\dot{u}_p + (D_1 + \Theta_1^T)u_p = D_1 u \tag{2.13}$$

where in addition to  $\Theta_1$ ,  $\Theta_2$  is an unknown parameter as well. This change in dynamics means that the the structure of the model used for control design is no longer accurate, and the autonomous controller may lose stability and command tracking ability. In particular, the challenge from the anomaly is the increase in relative degree between  $u$  and  $y_p$  from two to three.

In addition to an autonomous controller which generates control input  $u(t)$  in (2.12) and (2.13), a human supervisor is tasked with the high-level operation of the plant (2.11), including mission and task planning (commanding its mode of operation) and monitoring to ensure safe and anomaly-free operation. In this chapter, we consider *remote* human operators who cannot sense the vehicle state and dynamics directly through vestibular pathways. The human supervisor may be responsible for the supervision of multiple plant instances, as illustrated in Figure 2-1 for a highly flexible UAV platform. Operation is denoted *human-on-the-loop* in the same manner as the on-board human pilot considered in the problem of Section 2.1.

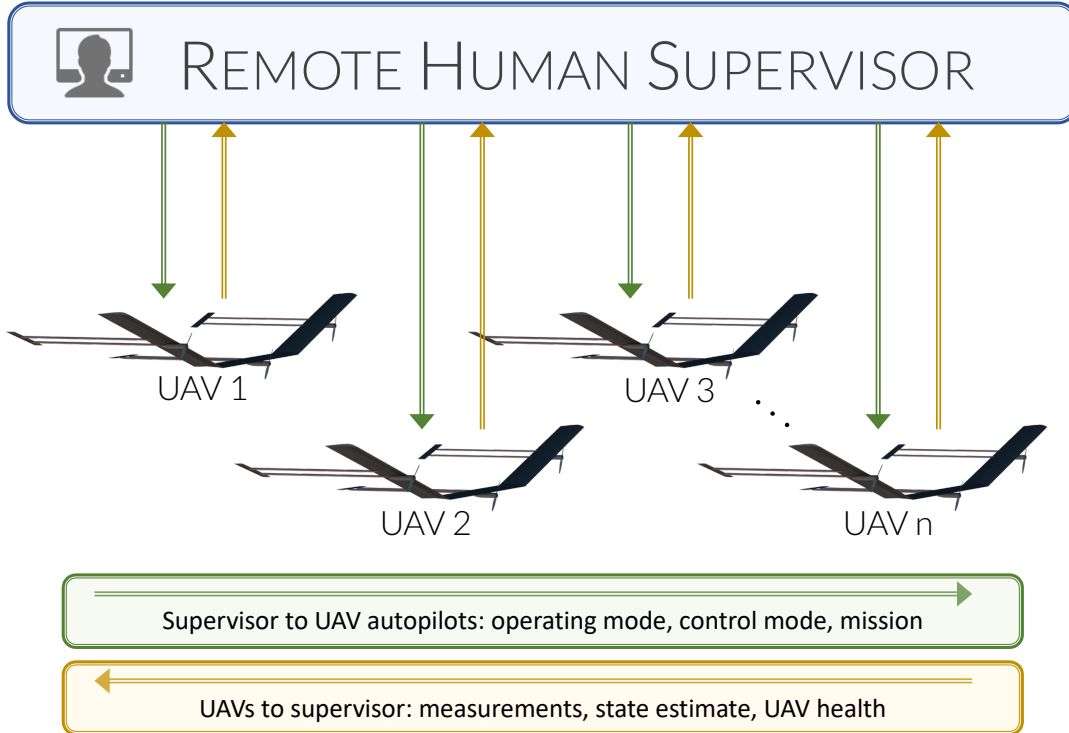


Figure 2-1: Supervisory operation of a fleet of high altitude, long endurance UAVs by remote human operator

It is assumed that the human supervisor has access to information on plant sensor measurements, state estimate, tracking performance, and health (via visual, haptic, and/or auditory interfaces), and is able to perceive changes in plant dynamics, such as an increased lag or decreased control effectiveness, via these interfaces. *Human-in-the-loop* operation is possible via remote controls, allowing the operator to actuate the plant by manually providing  $u(t)$  in (2.12) and (2.13). The sensing and actuation by the remote human supervisor include time delays  $\tau_s, \tau_a > 0$ , respectively.

The problem we investigate in Chapter 4 is whether the design of  $u(t)$  can be carried out using a shared decision-making and control architecture which combines

- (a) autonomous control methodologies
- (b) a remote human supervisor

so as to lead to a successful mitigation of an abrupt anomaly causing a change from (2.12) to (2.13) and restore tracking performance in the presence of uncertainty. This problem is a natural extension of the problem introduced in Section 2.1, where the solution must additionally accommodate

- (i) multi-input, multi-output plants;
- (ii) unmeasured state variables;
- (iii) remote human operators.

The shared control solution proposed in Chapter 4 of this thesis will thus build on the shared controller described in Chapter 3.

THIS PAGE INTENTIONALLY LEFT BLANK

# Chapter 3

## Shared Control with Human Pilot and State Feedback

In this chapter, we introduce a shared control architecture between human pilots and adaptive control algorithms to address the problems defined in Section 2.1. Adaptive controllers can be designed to permit autonomous control of the vehicle (2.1) in the presence of parametric uncertainties in  $A_p$  and  $B_p$ . On-board human pilots monitor the performance of the vehicle and are trained to manually control the vehicle in case of autopilot failure. Our shared anomaly response tasks the human pilot with providing key inputs based on higher-level perception of the anomaly, but delegates the low-level regulation and command tracking tasks to adaptive control algorithms which make use of these inputs. In Section 3.1, we describe two adaptive autopilot designs which in combination with the human operator whose precise role is described in Section 3.2, will solve the problem which was presented in Section 2.1. The overall shared control architecture is summarized in Section 3.3.

### 3.1 Full-State Feedback Adaptive Autopilot

Central to this work is the use of an autopilot which employs advanced control principles for low-level flight control tasks in the place of human pilots. In particular, our autopilot design uses adaptive control with the full vehicle state available for

feedback [24]. Closed-loop reference models (CRMs) [8] are utilized here to improve the transient performance of adaptive control, in comparison to open-loop reference models.

In this section, a *nominal* adaptive controller is designed to allow tracking of commands for the  $n$ th-order linear plant given in (2.1) when parameters of the plant model are uncertain, and – excluding exceptional failures – this is the controller to be used by the autopilot. A *recovery* adaptive controller is then designed for the  $(n+1)$ th-order system given in (2.5), which arises following an anomaly that changes the system dynamics. This recovery adaptive controller is not used under normal circumstances, but will form a part of the proposed shared control architecture used to address the problems which were stated in Section 2.1.

### 3.1.1 Nominal Adaptive Controller

The adaptive controller described in this section will be designed so as to produce a control input  $u(t)$  to the plant (2.1), of the form

$$u(t) = \theta(t)x_p(t) + q(t)r(t) \quad (3.1)$$

where  $\theta(t) \in \mathbb{R}^{1 \times n}$  is a vector of adaptive feedback gains on the plant state vector, and  $q(t)$  is a scalar adaptive feedforward gain on the external reference input (command),  $r(t)$ . The gains  $\theta(t)$  and  $q(t)$  will be adjusted online so that desired closed-loop command following behavior is achieved in the presence of uncertain plant parameters. The design of the adaptive controller is based upon the dynamics of a reference model, a dynamical system given by

$$\dot{x}_m(t) = A_m x_m(t) + B_m r(t) - L_m [x_p(t) - x_m(t)] \quad (3.2)$$

where  $A_m \in \mathbb{R}^{n \times n}$  is Hurwitz (real component of every eigenvalue is strictly negative),  $B_m \in \mathbb{R}^{n \times 1}$ ,  $L_m \in \mathbb{R}^{n \times n}$ , and  $e(t) \equiv x_p(t) - x_m(t)$  is defined as the state error. The matrix  $A_m$  can be designed using techniques such as the linear quadratic regulator

(LQR) method to model a desired closed-loop system dynamic response (i.e.  $A_m = \hat{A}_p - \hat{B}_p K_{\text{LQR}}$ , where  $\hat{A}_p$  and  $\hat{B}_p$  are *a priori* known estimates of uncertain  $A_p$  and  $B_p$ ). It is assumed that there exists scalar  $\lambda$  such that  $B_p \equiv \lambda B_m$ . The matrix  $L_m \neq 0$  differentiates this closed-loop reference model from an open-loop reference model.

With the plant, control law, and reference model dynamics defined in (2.1), (3.1), and (3.2), respectively, feedback gain  $\theta^*$  and feedforward gain  $q^*$  are defined by the following relations

$$A_p + B_p \theta^* = A_m \quad (3.3)$$

$$B_p q^* = B_m \quad (3.4)$$

and it is noted that when  $\theta(t) = \theta^*$  and  $q(t) = q^*$ , the closed-loop dynamics of the plant will match that of the reference model. These relations are referred to as the matching conditions of the adaptive controller.

Feedback and feedforward control gain adaptation is given by the adaptive laws

$$\dot{\theta}(t) = -\Gamma_\theta B_m^T P e(t) x_p^T(t) \quad (3.5)$$

$$\dot{q}(t) = -\gamma_q B_m^T P e(t) r(t) \quad (3.6)$$

where  $\Gamma_\theta > 0$  and  $\gamma_q > 0$  are a diagonal matrix and scalar, respectively, of constant weights. These weights correspond to learning rates on the feedback/feedforward parameters. The state error feedback gain,  $L_m$ , can be chosen to be

$$L_m = -A_m - \Gamma_\theta \quad (3.7)$$

which ensures that there exists positive definite matrix  $P > 0$ , the solution to the Lyapunov equation

$$(A_m + L_m)^T P + P(A_m + L_m) = -Q \quad (3.8)$$

for any positive definite matrix  $Q > 0$ .

To ensure robustness of the adaptive controller, a projection operator [28, 19]

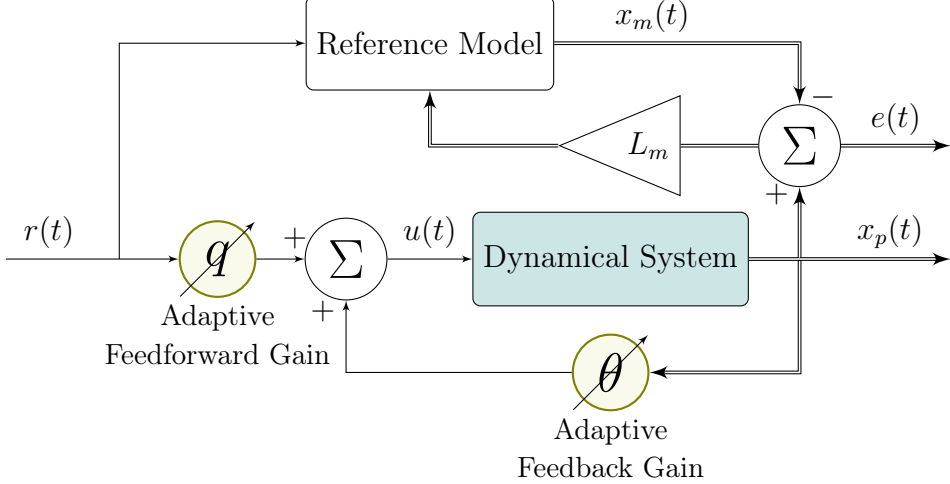


Figure 3-1: Block diagram of model reference adaptive controller with closed-loop reference model and full-state feedback

may be used in conjunction with the adaptive laws (3.5) and (3.6). The projection operator limits the magnitude of  $\dot{\theta}(t)$  and  $\dot{q}(t)$ , so that the parameters  $\theta(t)$  and  $q(t)$  remain within a convex set. Readers are referred to Ref. [8] for a detailed treatment of the projection operator as it applies to the general CRM-adaptive controller, but to summarize, the adaptive laws are modified from (3.5) and (3.6) to be

$$\dot{\theta}(t) = \text{Proj}(-\Gamma_\theta B_m^T P e(t) x_p^T(t), \theta(t)) \quad (3.9)$$

$$\dot{q}(t) = \text{Proj}(-\gamma_q B_m^T P e(t) r(t), q(t)) \quad (3.10)$$

with the vector projection operator defined as

$$\text{Proj}(Y, \Phi) = [\text{Proj}(y_1, \varphi_1) \dots \text{Proj}(y_n, \varphi_n)] \quad (3.11)$$

and the scalar projection operator defined as

$$\text{Proj}(y, \varphi) = \begin{cases} y(1 - f(\varphi)) & f(\varphi) > 0 \wedge y \nabla f(\varphi) > 0 \\ y & \text{otherwise} \end{cases} \quad (3.12)$$

The function  $f(\varphi)$  is taken to be

$$f(\varphi) = \frac{\varphi^2 - \varphi_m^2}{2\varphi_\epsilon\varphi_m + \varphi_\epsilon^2} \quad (3.13)$$

where  $\varphi_m$  and  $(\varphi_m + \varphi_\epsilon)$  define “soft” and “hard” bounds on the parameter  $\varphi$ , respectively.

With a plant given by (2.1), a control law defined as in (3.1), a reference model as in (3.2), and parameter adaptation as in (3.9) and (3.10), the goal of command tracking in the presence of parametric uncertainties is achieved. Section 3.1.2 describes a modification to the adaptive control design introduced in this section, which will constitute a portion of the shared control response to anomalies, as described in Section 2.1.

### 3.1.2 Recovery Adaptive Controller

The *recovery* adaptive controller here is designed using the same methods as that of the *nominal* adaptive controller described above, however it is designed based on a higher-order model of the plant, which is defined in (2.6). In order to satisfy the matching conditions for adaptive control given in (3.3) and (3.4), a corresponding higher-order reference model, accommodating additional state information, must be designed. The control law has the form

$$u(t) = \theta(t)x'_p(t) + q(t)r(t) \quad (3.14)$$

where  $x'_p \in \mathbb{R}^{n+1 \times 1}$  is the state of the plant augmented with first-order actuator dynamics, as in (2.6). The closed-loop reference model is then given by

$$\dot{x}'_m(t) = A'_m x'_m(t) + B'_m r(t) - L'_m [x'_p(t) - x'_m(t)]. \quad (3.15)$$

With a plant given by (2.6), a control law defined as in (3.14), a reference model as in (3.15), and parameter adaptation designed identically to (3.9) and (3.10) in the augmented state space, command tracking in the presence of parametric uncertainties

is achieved for the plant with first-order actuator dynamics (2.6). This adaptive controller is referred to as the recovery adaptive controller, as it will be used in conjunction with a human pilot in the proposed shared control framework to recover from dynamical anomalies.

## 3.2 Human Pilot

Trained human pilots develop internal models of the vehicle dynamics and expected performance in different situations, giving pilots a high level of situation awareness regarding the aircraft [4]. The idea of this shared decision-making and control architecture is to task the human pilot with responsibilities which require a high level of cognition in the shared response to an anomaly, in order to allow the use of the recovery adaptive autopilot described in Section 3.1.2 for low-level regulation and command tracking tasks following the anomaly.

The role of the human pilot in the shared controller is described as follows, as a sequence of responsibilities following the occurrence of an anomaly.

**Task 1.** Timely detection of anomalous closed-loop dynamical behavior

**Task 2.** Characterization of anomaly

**Task 3.** Commanding a change from nominal autopilot to recovery autopilot

The time when the anomaly occurs is denoted  $t := t_1^*$ , the time when the pilot completes the final task is denoted  $t := t_2^*$ , and the time at which irrecoverable failure would be reached without the pilot completing all tasks is denoted  $t := t_3^*$ . The human pilot must complete Tasks 1–3 such that  $t_2^* < t_3^*$  if a recovery is to be successful.

Completion of the first task requires that the on-board human pilot is able to perceive that something is wrong with the vehicle dynamics, and that deterioration in closed-loop performance is not caused by external disturbances or transient behavior in adaptation to uncertain parameters.

The second tasks requires the human pilot to understand more about the nature of the anomaly. For the anomaly considered in Section 2.1.1, the pilot must perceive

the additional lag in response to control inputs caused by the actuator anomaly. Even in a human-on-the-loop situation, when the pilot is not directly responsible for the generation of control input  $u(t)$ , anomalous vehicle behavior is expected to be manifested through changes in the closed-loop response of the vehicle and its disturbance-rejection abilities. Additionally, it is assumed that the pilot is able to perceive the autopilot’s control actions,  $u(t)$ , through visual displays or through kinesthetic or tactile feedback on the pilot’s controls [36, 38]. In combination with the pilot’s visual and vestibular sensing of vehicle dynamics, this sensing of autopilot control actions will allow the human pilot to determine the open-loop vehicle dynamics, in addition to the closed-loop dynamics, allowing for an enhanced perception and understanding of an anomaly. In the case of the anomaly considered in Section 2.1.2, the time-delayed sensor measurements would change the relationship between  $y_H$  and  $y_D$ , in addition to the closed-loop vehicle dynamics.

The final task involves the transfer of the pilot’s diagnosis to the autopilot, by changing the autopilot from its nominal adaptive control mode to the recovery adaptive control mode. We therefore hypothesize that an on-board human pilot has the sensory and perceptive capabilities necessary – with proper training – to carry out Tasks 1–3 in the presence of the anomalies described in Section 2.1.

### 3.3 Overall Shared Controller

The shared control algorithm between the adaptive autopilot and human pilot that we propose is as follows. Under nominal operating conditions, the adaptive controller as in (3.1), (3.9), and (3.10) is proposed. An anomaly is assumed to occur at  $t = t_1^*$ . Following this time instant, the pilot carries out Tasks 1–3 as in Section 3.2, and at  $t = t_2^*$  indicates to the adaptive autopilot the perceived increase in order. Using this pilot input, we propose an adaptive controller predicated on a higher-order dynamics of the open-loop plant (the recover adaptive controller) and assume that in addition to the plant output and its first  $n - 1$  time derivatives, the  $n$ th derivative with respect to time is measurable.

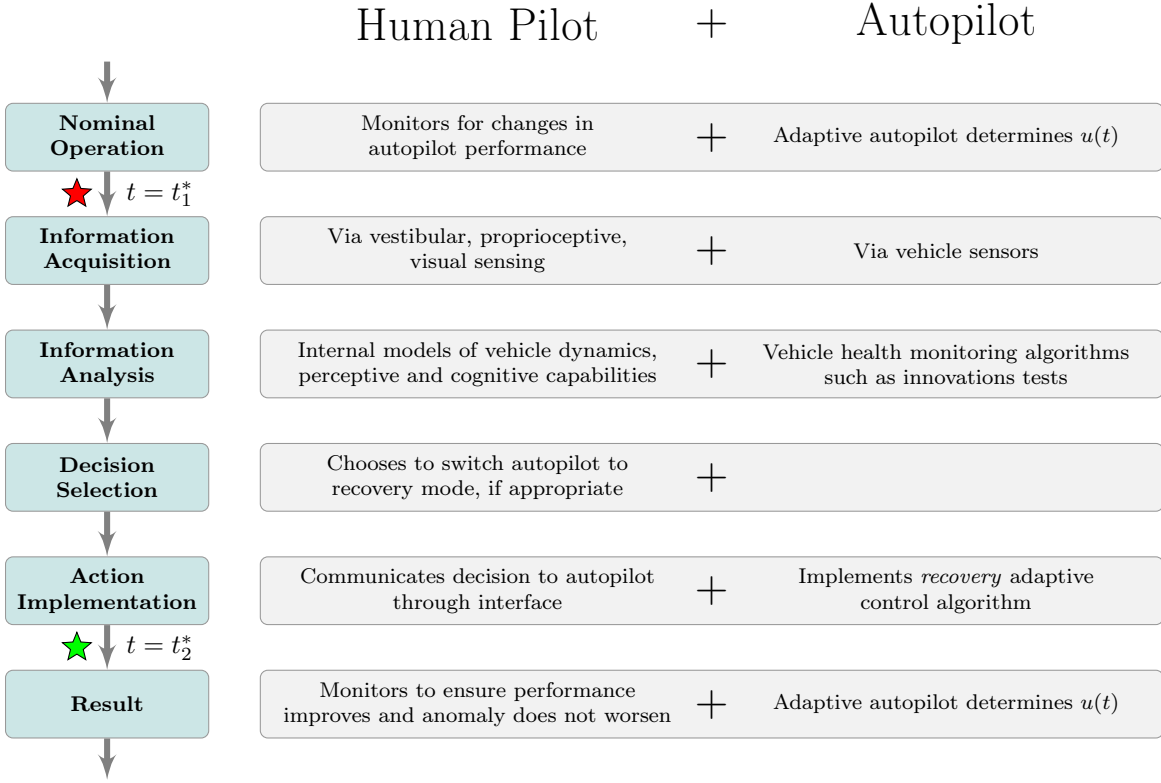


Figure 3-2: Proposed framework for shared decision-making and control between an on-board human pilot and adaptive control algorithms following an anomaly, with roles organized by stages of decision making as categorized in Ref. [26]

For the case of an actuator anomaly as in (2.4),  $\theta^* \in \mathbb{R}^3$  and  $q^*$  exist that solve the corresponding matching conditions in (3.3) and (3.4), and an adaptive controller as in (3.9) and (3.10) can be realized to lead to a stable closed-loop solutions and accurate tracking. These matching conditions are not met, however, in the case of the anomaly causing time-delayed sensor measurements (2.7). In the numerical examples, we will discuss the details of how such an adaptive controller with an increase in dimension following the pilot input performs for both cases of anomalies.

A detailed discussion of the stability of the resulting adaptive controller is not carried out in this thesis. But it is clear that if the time period  $(t_2^* - t_1^*)$  is sufficiently short compared to  $(t_3^* - t_1^*)$ , the adaptive controller will guarantee boundedness of the closed-loop system and convergence of  $e(t)$  to zero if our assumptions that the cause of the two anomalies results in an  $(n + 1)$ -order plant and that its full state vector is measurable are satisfied. Thus, if the human pilot carries out Tasks 1–3

sufficiently fast, the anomaly response based on this shared control architecture will restore closed-loop performance and stability in the presence of a sustained anomaly. We carry out detailed numerical simulation studies in Chapter 5 and evaluate the performance of this proposed shared control architecture in response to dynamical anomalies.

THIS PAGE INTENTIONALLY LEFT BLANK

# Chapter 4

## Shared Control with Remote Human Pilot and Output Feedback

In this chapter, a shared control framework is proposed to address the problem stated in Section 2.2. Whereas the shared control framework proposed in Chapter 3 was applicable to SISO plants with the full plant state measured and a human pilot on-board, the shared control framework to be presented here applies to MIMO plants where the full plant state is not measured directly, and humans operate remotely. As in Chapter 3, the shared control framework is designed so as to combine the merits of both adaptive control algorithms and humans.

It is assumed that adaptive autopilots and complementary higher-level motion planning algorithms allow for continuous autonomous operation of the vehicle in the presence of parametric uncertainties  $\Theta_p$ ,  $\Lambda_p$ , and  $\Theta_1$  in (2.11) and (2.12). Remote human operators monitor the performance of the vehicles and are trained and able to remotely pilot the vehicle in case of autopilot failure. The remote piloting of the vehicles, however, is a daunting task due to communication delays and a weakened understanding of the vehicle dynamics, state, and environment. Our shared anomaly response tasks the human operator with providing key inputs based on higher-level perception of the anomaly, but delegates the low-level regulation and command tracking tasks to adaptive control algorithms which make use of these inputs. In Section 4.1, we describe two adaptive autopilot designs which in combination with the human

operator whose precise role is described in Section 4.2, will solve the problem which was presented in Section 2.2. The overall shared control architecture is summarized in Section 4.3.

## 4.1 Output Feedback Adaptive Autopilot

In this section, an autonomous controller is designed so that plant outputs  $z_p(t)$  in (2.11) will track prescribed commands  $z_{cmd}(t)$ . The shared control framework will make use of separate adaptive control designs for the plant (2.11) in combination with actuator dynamics (2.12) and (2.13). The control design accommodating first-order actuators is denoted the *nominal* adaptive control design, and excluding exceptional failures, is the controller in use by the autopilot. The control design accommodating second-order actuators is a predefined *recovery* adaptive controller, whose use case will be defined more fully in Section 4.2. To achieve the control goals stated in Section 2, control design consists of

- (i) baseline control design using the robust servomechanism linear quadratic regulator method (RSLQR or LQR-PI [20]);
- (ii) adaptive output-feedback augmentation for parametric uncertainties in the plant.

Control design in each case uses an augmented linear plant formulation, where the plant (2.11) is extended with the actuator dynamics – either (2.12) or (2.13) – as well as integrated tracking errors

$$e_z^T(t) = \int_0^t (z_p(\tau) - z_{cmd}(\tau)) d\tau. \quad (4.1)$$

The augmented plant model with state vector  $x = \begin{bmatrix} x_p^T & x_{act}^T & (e_z^T)^T \end{bmatrix}^T$  can be written compactly as

$$\begin{aligned} \dot{x} &= (A + B_1 \Psi_1^T + B_r \Psi_r^T) x + B_r \Lambda u + B_z z_{cmd} \\ y &= Cx, \quad z = C_z x \end{aligned} \quad (4.2)$$

where  $x \in \mathbb{R}^n$ ,  $u \in \mathbb{R}^m$ ,  $y \in \mathbb{R}^p$  are redefined states, inputs and outputs, respectively. This plant has unknown matrices  $\Psi_1$ ,  $\Psi_r$ , and  $\Lambda$ , which contain plant uncertainties ( $\Theta_p$ ), actuator uncertainties ( $\Theta_i$  in (2.12) and (2.13)), and control effectiveness ( $\Lambda_p$ ), respectively. Note that the uncertainty has been reparameterized for notational simplicity when analyzing the augmented plant form. The exact forms of  $B_r$  and  $\Psi_r$  depend on whether the actuators are first-order (2.12) or second-order (2.13), and the subscript  $r$  indicates the relative degree of the augmented plant. It is noted that the augmented plant model which arises from the inclusion of actuator model (2.12) in the plant (2.11) has relative degree two, while the augmented plant model associated with the inclusion of actuator model (2.13) has relative degree three.

For adaptive control design, closed-loop reference models [8] are designed as

$$\dot{x}_m = A_m x_m + B_z z_{cmd} + L e_y + \mathcal{F}_r(t), \quad y_m = C x_m \quad (4.3)$$

where  $e_y(t) = y(t) - y_m(t)$ ,  $A_m = A - B_r K_{\text{LQR}}^T$  with  $K_{\text{LQR}} \in \mathbb{R}^{n \times m}$  is a baseline feedback control gain designed for the system without uncertainty using RSLQR, as described by [20].  $L$  is a Luenberger-like feedback gain, and  $\mathcal{F}_r(t)$  is a function used for plants having  $r \geq 2$  to recover stability guarantees in the presence of uncertainty. Note that  $u^*(t) = -K_{\text{LQR}}^T x(t)$  is the control policy which minimizes the infinite-horizon quadratic cost function

$$J = \int_0^\infty [x^T Q_{\text{LQR}} x + u^T R_{\text{LQR}} u] dt \quad (4.4)$$

where  $Q \geq 0$  and  $R > 0$ , and the system dynamics are assumed to be  $\dot{x} = Ax + B_r u$ .

In what follows, we define a *nominal* adaptive autopilot for the plant (4.2) as one that successfully accommodates actuator dynamics in the form of (2.12) and unknown  $\Theta_p$ ,  $\Theta_1$ , and  $\Lambda_p$ . We define a *recovery* adaptive autopilot to be one that is successful in accommodating actuator dynamics (2.13), i.e., when it is known that the relative degree is three, with uncertain parameters  $\Theta_p$ ,  $\Theta_1$ ,  $\Theta_2$ , and  $\Lambda_p$ . We restrict our attention in this chapter to augmented plant models (4.2) which are square (i.e. the number of inputs,  $m$ , is equal to the number of outputs,  $p$ ). For details of closed-loop

stability guarantees with the nominal and recovery adaptive controllers, readers are referred to [31] and [29], respectively.

#### 4.1.1 Nominal Adaptive Controller

The control design for the plant with first-order actuator dynamics will be summarized by describing the CRM residual gain matrix  $L$ , function  $\mathcal{F}_2(t)$ , control law  $u(t)$ , and parameter adaptation. Note that  $B_2$  represents  $B_r$  from (4.2) and  $\mathcal{F}_2(t)$  represents  $\mathcal{F}_r(t)$  from (4.3) for this relative degree two plant.

The feedback matrix  $L$  is designed as follows. We define the “relative degree one input path”

$$B_1^a = \alpha_0 B_2 + \alpha_1 A B_2 \quad (4.5)$$

where  $\alpha_i > 0$  are free design parameters. We then define

$$S = (CB_1^a)^T \quad (4.6)$$

$$\bar{C} = SC \quad (4.7)$$

$$R^{-1} = (\bar{C}B_1^a)^{-1} [\bar{C}AB_1^a + (\bar{C}AB_1^a)^T](\bar{C}B_1^a)^{-1} + \epsilon I \quad (4.8)$$

$$L = B_1^a R^{-1} S \quad (4.9)$$

where the scalar parameter  $\epsilon > 0$  [30, Eq. 30] is chosen to be large enough in magnitude to guarantee stability of the adaptive system.

The function  $\mathcal{F}_2(t)$  makes use of scaled output error signal

$$e_{sy}(t) = R^{-1} S e_y(t) \quad (4.10)$$

and a filtered version of this signal, denoted  $\bar{e}_{sy}(t)$ , given in the form of a differential equation as

$$(\alpha_0 + \alpha_1 \frac{d}{dt}) \{\bar{e}_{sy}(t)\} = \alpha_1 e_{sy}(t). \quad (4.11)$$

It is worth noting that this filtered signal can be represented in the Laplace  $s$ -domain

as

$$\bar{E}_{sy}(s) = \frac{\alpha_1}{\alpha_1 s + \alpha_0} E_{sy}(s).$$

The function  $\mathcal{F}_2(t)$ , which is used to ensure stability of the overall adaptive system, is then defined as

$$\mathcal{F}_2(t) = B_2(\alpha_0 + \alpha_1 \frac{d}{dt}) \{ \hat{\Psi}_m^T(t) \bar{e}_{sy}(t) \} \quad (4.12)$$

where  $\hat{\Psi}_m(t)$  is a matrix of adaptive parameters. Similar to (4.11), we define filtered reference model state,  $\bar{x}_m(t)$ , with the differential equation

$$(\alpha_0 + \alpha_1 \frac{d}{dt}) \{ \bar{x}_m(t) \} = \alpha_1 x_m(t) \quad (4.13)$$

and the equivalent frequency domain representation

$$\bar{X}_m(s) = \frac{\alpha_1}{\alpha_1 s + \alpha_0} X_m(s). \quad (4.14)$$

We define a regressor vector of known signals as

$$\mathcal{X}(t) = [(K_{LQR}^T \bar{x}_m)^T, \quad x_m^T, \quad \bar{x}_m^T]^T. \quad (4.15)$$

The control law which defines the input  $u(t)$  to the plant (4.2), is then given by

$$u(t) = -(\alpha_0 + \alpha_1 \frac{d}{dt}) \{ \hat{\Psi}_\Lambda^T(t) \mathcal{X}(t) \} \quad (4.16)$$

where  $\hat{\Psi}_\Lambda(t)$  is a matrix of adaptive parameters. The laws for adaptation of parameter matrices  $\hat{\Psi}_m(t)$  and  $\hat{\Psi}_\Lambda(t)$  are given by

$$\begin{aligned} \dot{\hat{\Psi}}_m(t) &= \Gamma_m \bar{e}_{sy}(t) e_y^T(t) S^T \\ \dot{\hat{\Psi}}_\Lambda(t) &= -\Gamma_\Lambda \mathcal{X}(t) e_y^T(t) S^T \end{aligned} \quad (4.17)$$

with diagonal adaptation gains  $\Gamma_m, \Gamma_\Lambda > 0$ . We note that the derivatives of the adaptive parameters, computed in (4.17), are used to implement (4.12) and (4.16) with the product rule of differentiation. The expanded form of the control law,

following the product rule of differentiation, is given by

$$u(t) = -\alpha_0 \hat{\Psi}_\Lambda^T(t) \mathcal{X}(t) - \alpha_1 \dot{\hat{\Psi}}_\Lambda^T(t) \mathcal{X}(t) - \alpha_1 \hat{\Psi}_\Lambda^T(t) \dot{\mathcal{X}}(t). \quad (4.18)$$

For the plant (2.11) with first-order actuator model (2.12), an adaptive controller designed with reference model given by (4.3), control input given by (4.16), and parameter adaptation given by (4.17), asymptotic convergence of  $e_y(t)$  to 0 is achieved.

#### 4.1.2 Recovery Adaptive Controller

Control design for the plant (2.11) with the second-order actuator model (2.13) is similar to that described above, but requires modifications to ensure strict positive realness of the transfer matrix of the model-following error dynamics.

The definition of  $L$  is modified by replacing  $B_1^a$  in (4.5) with

$$B_1^a = \alpha_0 B_3 + \alpha_1 A B_3 + \alpha_2 A^2 B_3 \quad (4.19)$$

and proceeding with (4.6)–(4.9). A definition for  $\epsilon > 0$  in this case can be found in [29]. To simplify notation, the operator  $\Pi\{\cdot\}$  is defined as

$$\Pi\{\cdot\} = \left( \alpha_0 + \alpha_1 \frac{d}{dt} + \alpha_2 \frac{d^2}{dt^2} \right) \{\cdot\}. \quad (4.20)$$

The function  $\mathcal{F}_3(t)$  utilizes several filtered output error vectors, denoted  $\bar{e}_{sy}^{[1]}(t)$ ,  $\bar{e}_{sy}^{[2]}(t)$ , and  $\bar{e}_{sy}^{[1][2]}(t)$ , defined by the differential equations

$$\begin{aligned} \Pi\{\bar{e}_{sy}^{[1]}(t)\} &= (\alpha_1 + \alpha_2 \frac{d}{dt}) \{e_{sy}(t)\} \\ \Pi\{\bar{e}_{sy}^{[2]}(t)\} &= \alpha_2 e_{sy}(t) \\ \Pi\{\bar{e}_{sy}^{[1][2]}(t)\} &= (\alpha_2 \frac{d}{dt}) \{\hat{\phi}_1^T(t) \bar{e}_{sy}^{[1]}(t)\} \end{aligned} \quad (4.21)$$

where  $e_{sy}(t)$  was defined in (4.10),  $\hat{\phi}_1(t)$  is a vector of adaptive parameters, and coefficients  $\alpha_i > 0$  are free design parameters. The equivalent frequency domain

representations of these filtered signals are given by

$$\begin{aligned}\bar{E}_{sy}^{[1]}(s) &= \frac{\alpha_2 s + \alpha_1}{\alpha_2 s^2 + \alpha_1 s + \alpha_0} E_{sy}(s), & \bar{E}_{sy}^{[1]}(s) &= \frac{\alpha_2}{\alpha_2 s^2 + \alpha_1 s + \alpha_0} E_{sy}(s) \\ \bar{E}_{sy}^{[1][2]}(s) &= \frac{\alpha_2 s}{\alpha_2 s^2 + \alpha_1 s + \alpha_0} (\hat{\phi}_1^T(s) E_{sy}^{[1]}(s))\end{aligned}\quad (4.22)$$

We define a scaled, integrated measurement output error,

$$e_y^{\mathcal{I}}(t) = \int_0^t L(y(\tau) - y_m(\tau)) d\tau \quad (4.23)$$

which is used to define filtered error signals  $\bar{e}_{\mathcal{I}y}^{[1]}(t)$  and  $\bar{e}_{\mathcal{I}y}^{[1][2]}(t)$ , given by

$$\begin{aligned}\Pi\{\bar{e}_{\mathcal{I}y}^{[1]}(t)\} &= (\alpha_1 \frac{d}{dt} + \alpha_2 \frac{d^2}{dt^2}) \{\hat{\Phi}_1^T(t) e_y^{\mathcal{I}}(t)\} \\ \Pi\{\bar{e}_{\mathcal{I}y}^{[1][2]}(t)\} &= (\alpha_2 \frac{d}{dt}) \{\hat{\Lambda}^T(t) \bar{e}_{\mathcal{I}y}^{[1]}(t)\}\end{aligned}\quad (4.24)$$

where  $\hat{\Phi}_1(t)$  and  $\hat{\Lambda}(t)$  are matrices of adaptive parameters. We define operators

$$\begin{aligned}f_a\{\cdot\} &= (\alpha_0 \alpha_2 B_3 + (\alpha_1 B_3 + \alpha_2 A B_3) \frac{d}{dt}) \{\cdot\} \\ f_b\{\cdot\} &= \alpha_2 B_3 \Pi\{\cdot\}\end{aligned}\quad (4.25)$$

and use these to fully define

$$\begin{aligned}\mathcal{F}_3(t) &= f_a \{\hat{\phi}_1^T(t) \bar{e}_{sy}^{[1]}(t) - \hat{\Lambda}^T(t) \bar{e}_{\mathcal{I}y}^{[1]}(t)\} \\ &\quad + f_b \{\hat{\phi}_1^T(t) [\bar{e}_{sy}^{[1][2]}(t) - \bar{e}_{\mathcal{I}y}^{[1][2]}(t)] + \hat{\phi}_2^T(t) \bar{e}_{sy}^{[2]}(t)\}\end{aligned}\quad (4.26)$$

where  $\hat{\phi}_2(t)$  is an additional vector of adaptive parameters. The control input synthesized by the recovery adaptive controller, as well as parameter adaptation, make use of filtered reference model states  $\bar{x}_m^{[1]}$  and  $\bar{x}_m^{[2]}$ , given by the differential equations

$$\begin{aligned}\Pi\{\bar{x}_m^{[1]}(t)\} &= (\alpha_1 + \alpha_2 \frac{d}{dt}) \{x_m(t)\} \\ \Pi\{\bar{x}_m^{[2]}(t)\} &= \alpha_2 x_m(t).\end{aligned}\quad (4.27)$$

Variable  $\bar{v}_m(t)$  is introduced, with artificial time derivatives, such that

$$\begin{aligned}\bar{v}_m &= x_m, \quad \frac{d}{dt}\{\bar{v}_m\} = Ax_m + B_z z_{cmd} \\ \frac{d^2}{dt^2}\{\bar{v}_m\} &= A^2 x_m + AB_z z_{cmd} + B_z \frac{dz_{cmd}}{dt} - AL e_y.\end{aligned}\tag{4.28}$$

The regressor vector  $\mathcal{X}(t)$ , similar to that used by the nominal adaptive controller, is defined as

$$\mathcal{X}(t) = [(K_{LQR}^T \bar{x}_m^{[2]})^T, \quad \bar{v}_m^T, \quad \bar{x}_m^{[1]T}, \quad \bar{x}_m^{[2]T}]^T.\tag{4.29}$$

The control law  $u(t)$  for the recovery adaptive controller is

$$\begin{aligned}u(t) &= -\Pi\{\hat{\Psi}^T(t)\mathcal{X}(t)\} \\ &\quad -(\alpha_1 \frac{d}{dt} + \alpha_2 \frac{d^2}{dt^2})\{\hat{\Phi}_1^T(t)\}e_y^T(t)\end{aligned}\tag{4.30}$$

where

$$\hat{\Psi}(t) = [\hat{\Upsilon}^T(t), \quad \hat{\Phi}_1^T(t), \quad \hat{\Phi}_2^T(t), \quad \hat{\Phi}_3^T(t)]^T\tag{4.31}$$

is a matrix of adaptive parameters.

In this controller, the laws for parameter adaptation use second-order tuners as in [29]. This differs from the first-order adaptive laws used in the nominal adaptive control design, and in the adaptive controllers defined in Chapter 3. We first define a regressor vector  $\nu(t)$  of filtered error signals

$$\nu(t) = \left[(\bar{e}_{sy}^{[1][2]} - \bar{e}_{sy}^{[1]} - \bar{e}_{sy}^{[1][2]})^T, \quad (-\bar{e}_{sy}^{[2]})^T, \quad (\bar{e}_{sy}^{[1]})^T\right]^T\tag{4.32}$$

and associated matrix of adaptive parameters

$$\hat{\Theta}(t) = [\hat{\phi}_1^T(t), \quad \hat{\phi}_2^T(t), \quad \hat{\Lambda}^T(t)]^T.\tag{4.33}$$

Inputs to the second-order tuners are calculated by integrating

$$\begin{aligned}\dot{\hat{\Psi}}'(t) &= \Gamma_\Psi \mathcal{X} e_y^T S^T \text{sgn}(\Lambda) \\ \dot{\hat{\Theta}}'(t) &= -\Gamma_\Theta \nu e_y^T S^T\end{aligned}\tag{4.34}$$

where  $\Gamma_\Psi, \Gamma_\Theta > 0$  are diagonal adaptation gains and the  $(\cdot)'$  notation is used to differentiate these tuner inputs from the adaptive parameters which are the tuner outputs. The desired matrices of adaptive parameters are outputs of the tuners

$$\begin{aligned}\dot{X}_{\hat{\Psi}}(t) &= (A_T X_{\hat{\Psi}} + B_T (\hat{\Psi}'(t))^T) g(\mathcal{X}, \mu_{\mathcal{X}}) \\ \hat{\Psi}(t) &= (C_T X_{\hat{\Psi}})^T \\ \dot{X}_{\hat{\Theta}}(t) &= (A_T X_{\hat{\Theta}} + B_T (\hat{\Theta}'(t))^T) g(\nu, \mu_{\nu}) \\ \hat{\Theta}(t) &= (C_T X_{\hat{\Theta}})^T\end{aligned}\tag{4.35}$$

where

$$g(\mathbf{x}, \mu) = 1 + \mu \mathbf{x}^T \mathbf{x}\tag{4.36}$$

is a time-varying gain with scalar gain  $\mu$  described in [29].  $A_T \in \mathbb{R}^{2m \times 2m}$ ,  $B_T \in \mathbb{R}^{2m \times m}$ , and  $C_T \in \mathbb{R}^{m \times 2m}$  are block diagonal matrices with diagonal blocks

$$A_{T,i} = \begin{bmatrix} 0 & 1 \\ -\frac{\alpha_0}{\alpha_2} & -\frac{\alpha_1}{\alpha_2} \end{bmatrix}, \quad B_{T,i} = \begin{bmatrix} 0 \\ \frac{\alpha_0}{\alpha_2} \end{bmatrix}, \quad C_{T,i} = \begin{bmatrix} 1 & 0 \end{bmatrix}.\tag{4.37}$$

Derivatives of the adaptive parameters, used in (4.21), (4.24), (4.26), and (4.30), are given by

$$\begin{aligned}\dot{\hat{\Psi}}(t) &= (C_T^\delta X_{\hat{\Psi}})^T, & \ddot{\hat{\Psi}}(t) &= (C_T^{\delta\delta} X_{\hat{\Psi}})^T \\ \dot{\hat{\Theta}}(t) &= (C_T^\delta X_{\hat{\Theta}})^T, & \ddot{\hat{\Theta}}(t) &= (C_T^{\delta\delta} X_{\hat{\Theta}})^T\end{aligned}\tag{4.38}$$

where  $C_T^\delta, C_T^{\delta\delta} \in \mathbb{R}^{m \times 2m}$  are block diagonal matrices with diagonals  $C_{T,i}^\delta = [0, 1]$  and  $C_{T,i}^{\delta\delta} = -\frac{1}{\alpha_2} [\alpha_0, \alpha_1]$ . For the plant (2.11) with second-order actuator model (2.13), an adaptive controller designed with reference model given by (4.3), control input given by (4.30), and parameter adaptation given by (4.34)–(4.38), asymptotic convergence of  $e_y(t)$  to 0 is achieved.

## 4.2 Remote Human Pilot

We task the remote human supervisor with the following three responsibilities for shared anomaly response.

**Task 1.** Timely detection of anomalous closed-loop dynamical behavior

**Task 2.** Isolation and characterization of anomaly

**Task 3.** Commanding a change from nominal autopilot (4.5)–(4.17) to recovery autopilot (4.19)–(4.38)

The first task requires an attentive human operator able to discern that

- (a) an anomaly has occurred and control performance degradation is not caused solely by external disturbances;
- (b) swift action must be taken in order to recover stability and performance;
- (c) it may be possible to recover stability and performance via corrective action.

For the second task, the human operator must

- (a) understand which control loop (e.g. pitch mode, roll mode, airspeed, in a fixed-wing UAV application) is affected by anomaly;
- (b) perceive an increased lag in plant response to commands.

The final task for the trained remote human operator is the transfer of this diagnosis to the autopilot, by changing the relevant controller to its recovery mode.

## 4.3 Overall Shared Controller

The shared control architecture between adaptive autopilots and a human operator that we propose is as follows. Before the occurrence of an anomaly, the nominal adaptive autopilot with control action defined in (4.16) is used to control the plant. An anomaly which abruptly changes actuator dynamics from (2.12) to (2.13) is assumed

to occur at  $t := t_1^*$ . Following this time instant, the human operator is responsible for carrying out tasks 1–3 before the time limit at which failure would occur without action ( $t := t_3^*$ ). The completion of task 3 by the human ( $t := t_2^*$ ) results in a switch to the recovery adaptive autopilot with control action as in (4.30).

Note that our shared control architecture does not involve a handover of regulation and command tracking tasks to the human following an anomaly. Instead, in our shared control architecture, the human operator is responsible for high-level cognition tasks while adaptive autopilots retain responsibility for low-level regulation, therefore directly leveraging and combining their complementary merits.

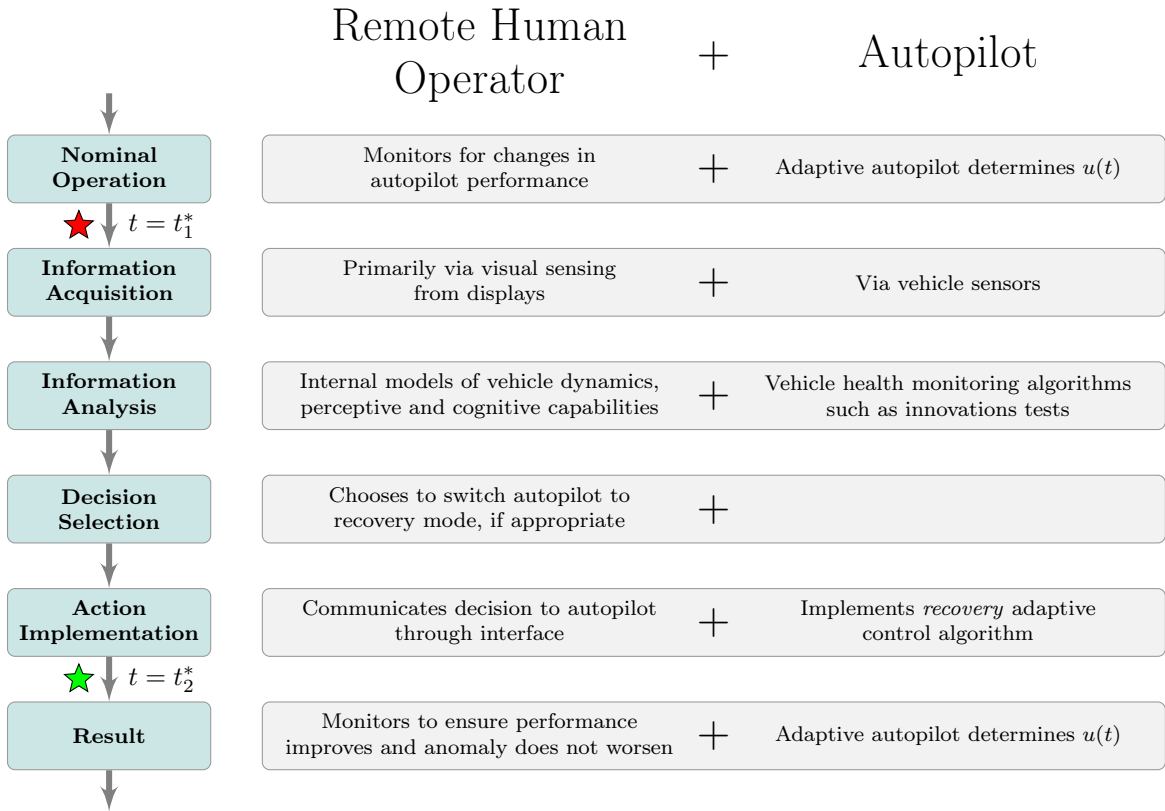


Figure 4-1: Proposed framework for shared decision-making and control between a remote human operator and adaptive control algorithms following an anomaly, with roles organized by stages of decision making as categorized in Ref. [26]

A detailed discussion of the stability of the closed-loop system with the overall shared controller is not carried out in this paper. But it is clear that if the human completes tasks 1–3 sufficiently fast (i.e.,  $t_2^* < t_3^*$ ), then the shared controller will guar-

antee boundedness of the closed-loop system and convergence of  $e(t) = x(t) - x_m(t)$  to zero if our assumptions are satisfied. We carry out detailed numerical simulations in the following chapter and evaluate the performance of the shared controller proposed above.

# Chapter 5

## Simulated Anomaly Response Scenarios

### 5.1 SISO State Feedback and On-Board Pilot

The shared control solution introduced in Chapter 3 is applied to the problem introduced in Section 2.1, using a simulation model of the lateral-directional dynamics of a fixed-wing aircraft and making assumptions about the perceptive capabilities and actions of an on-board human pilot. The aircraft model used in simulation is described in Section 5.1.1. The results of numerical simulations of the control of this plant and recovery from the two anomalies – actuators whose dynamics change abruptly from a DC gain to first-order, and sensors whose measurements abruptly become time-delayed – are presented in Sections 5.1.2 and 5.1.3, respectively.

#### 5.1.1 Aircraft Rolling Mode Dynamics

This section describes the lateral-directional dynamics of a fixed-wing aircraft. For an aircraft in steady wings-level flight with equilibrium speed  $V_0$ , pitch angle  $\theta_0$ , and no sideslip ( $\beta_0 = 0$ ), and assuming small perturbations about the equilibrium point, the lateral-directional dynamics of the aircraft can be decoupled from the longitudinal

aircraft dynamics, and linearized as follows [35]:

$$\underbrace{\begin{bmatrix} \dot{\beta} \\ \dot{\phi}_s \\ \dot{p}_s \\ \dot{r}_s \end{bmatrix}}_{\dot{x}_{\text{lat}}} = \underbrace{\begin{bmatrix} \frac{Y_\beta}{V_0} & \frac{g_D \cos \theta_0}{V_0} & \frac{Y_p}{V_0} & \frac{Y_r}{V_0} - 1 \\ 0 & 0 & \frac{1}{\cos \theta_0} & 0 \\ L_\beta & 0 & L_p & L_r \\ N_\beta & 0 & N_p & N_r \end{bmatrix}}_{A_{\text{lat}}} \underbrace{\begin{bmatrix} \beta \\ \phi_s \\ p_s \\ r_s \end{bmatrix}}_{\dot{x}_{\text{lat}}} + \underbrace{\begin{bmatrix} \frac{Y_{\delta_a}}{V_0} & \frac{Y_{\delta_r}}{V_0} \\ 0 & 0 \\ L_{\delta_a} & L_{\delta_r} \\ N_{\delta_a} & N_{\delta_r} \end{bmatrix}}_{B_{\text{lat}}} \underbrace{\begin{bmatrix} \delta_a \\ \delta_r \end{bmatrix}}_{u_{\text{lat}}} \quad (5.1)$$

where derivations of the stability and control derivatives in matrices  $A_{\text{lat}}$  and  $B_{\text{lat}}$  can be found in other references (see Refs. [35] or [20] for more details). The states correspond to sideslip angle, stability axis bank angle, stability axis roll rate, and stability axis yaw rate, respectively, while the control inputs correspond to aileron and rudder deflections.

Based on time-scale separation, second-order dynamics of aileron-to-roll-angle are extracted from this fourth-order system and denoted here as the rolling mode dynamics, given by

$$\underbrace{\begin{bmatrix} \dot{\phi} \\ \dot{p} \end{bmatrix}}_{\dot{x}_p} = \underbrace{\begin{bmatrix} 0 & 1 \\ 0 & L_p \end{bmatrix}}_{A_p} \underbrace{\begin{bmatrix} \phi \\ p \end{bmatrix}}_{x_p} + \underbrace{\begin{bmatrix} 0 \\ L_{\delta_a} \end{bmatrix}}_{B_p} \underbrace{\begin{bmatrix} \delta_a \\ u_p \end{bmatrix}}_{u_{\text{lat}}}. \quad (5.2)$$

This system corresponds to the plant as in (2.1), and it is noted that the rolling mode dynamics has the following transfer function in the Laplace frequency domain:

$$\frac{\Phi(s)}{\Delta_a(s)} = \frac{L_{\delta_a}}{s^2 - L_p s}. \quad (5.3)$$

In these equations,  $\delta_a$  represents aileron input, and  $\phi$  and  $p$  denote the aircraft bank angle and roll rate in stability axes, with the subscript  $(\cdot)_s$  dropped for notational simplicity. It is assumed that the state vector  $(x_p)$  is fully available for feedback (directly from sensors for  $p$ , and via integration of  $p$  for  $\phi$ ).  $L_p$  is the roll damping derivative and  $L_{\delta_a}$  is the rolling moment due to aileron deflection. We consider scenarios in which these parameters may be unknown, but are addressed in normal operation by an adaptive autopilot. The system has been simplified by fixing

$\delta_r(t) = 0$  (no rudder input), so that aileron deflection is the only input. In normal operation, we assume the vehicle has sufficiently fast actuators, so that  $\delta_a(t) = u(t)$  and equivalently  $\Delta_a(s) = U(s)$ , where  $u(t)$  is the control signal.

Under nominal vehicle operation with the plant given by (5.2), a second-order reference model corresponding to (3.2) is used

$$\underbrace{\begin{bmatrix} \dot{\phi}_d \\ \dot{p}_d \end{bmatrix}}_{\dot{x}_m} = \underbrace{\begin{bmatrix} 0 & 1 \\ -a_{m,1} & -a_{m,2} \end{bmatrix}}_{A_m} \underbrace{\begin{bmatrix} \phi_d \\ p_d \end{bmatrix}}_{x_m} + \underbrace{\begin{bmatrix} 0 \\ b_{m,2} \end{bmatrix}}_{B_m} r(t) - L_m e(t) \quad (5.4)$$

where  $x_m(t)$  is the CRM state vector,  $e(t) = x_p(t) - x_m(t)$  is the model-following error, and  $r(t)$  is the commanded bank angle. It is straightforward to see that a choice of

$$\theta^* = \left[ \frac{-a_{m,1}}{L_{\delta_a}} \quad \frac{-a_{m,2} - L_p}{L_{\delta_a}} \right] \quad (5.5)$$

$$q^* = \frac{b_{m,2}}{L_{\delta_a}} \quad (5.6)$$

solves the matching condition in (3.3) and (3.4). This in turn implies that even if the roll damping derivative ( $L_p$ ) and the rolling moment due to aileron deflection ( $L_{\delta_a}$ ) are unknown, the adaptive controller in (3.1), (3.9), and (3.10) will be able to vary the feedback and feedforward gains such that the closed-loop response of the system is satisfactory. We shall denote such a case as nominal operation, and consider the anomalous cases as those where in addition to parametric uncertainties, changes in dynamics as described in Sections 2.1.1 and 2.1.2 occur.

Numerical data for a Boeing 747 model flying straight-and-level at Mach 0.25 at sea level [9] is substituted into (5.2) to define the nominal model of plant dynamics used in simulation,

$$\underbrace{\begin{bmatrix} \dot{\phi} \\ \dot{p} \end{bmatrix}}_{\dot{x}_p} = \underbrace{\begin{bmatrix} 0 & 1 \\ 0 & -1.10 \end{bmatrix}}_{A_p} \underbrace{\begin{bmatrix} \phi \\ p \end{bmatrix}}_{x_p} + \underbrace{\begin{bmatrix} 0 \\ 0.318 \end{bmatrix}}_{B_p} \delta_a \quad (5.7)$$

which results in the open-loop transfer function

$$\frac{\Phi(s)}{\Delta_a(s)} = \frac{0.318}{s^2 + 1.10s}. \quad (5.8)$$

A closed-loop reference model, corresponding to (5.4), is designed with the following numerical values

$$\dot{x}_m = \underbrace{\begin{bmatrix} 0 & 1 \\ -8 & -6 \end{bmatrix}}_{A_m} x_m + \underbrace{\begin{bmatrix} 0 \\ 8 \end{bmatrix}}_{B_m} r - \underbrace{\begin{bmatrix} -10 & -1 \\ 8 & -4 \end{bmatrix}}_{L_m} e \quad (5.9)$$

for use with the nominal adaptive controller. The initial feedback and feedforward parameters used in simulation,  $\theta(t = 0)$  and  $q(t = 0)$ , are chosen such that the matching conditions of (5.5) and (5.6) are met.

The two cases of anomalies discussed in Sections 2.1.1 and 2.1.2, of the introduction of actuator dynamics and a time delay in state measurement, respectively, were simulated numerically using MATLAB/Simulink for bank angle tracking tasks. In these simulations, the commanded stability axis bank angle is a sequence of 5-second steps. In the simulations of these two types of anomalies, which are presented in Sections 5.1.2 and 5.1.3, the anomaly is assumed to occur at  $t_1^* = 30\text{s}$ , and the corrective action is applied to the controller at  $t_2^* = 90\text{s}$ . Time  $t_3^*$  denotes the time when failure of the aircraft is assumed to occur, if applicable. The three anomaly response (AR) simulations to be presented are summarized as follows.

**Act-AR (Shared)** Simulation of a shared control response to an anomaly which causes a plant with parametric uncertainties to abruptly undergo a change in actuator dynamics from direct gain to first-order lag

**Del-AR (Shared)** Simulation of a shared control response to an anomaly which introduces a time delay into the measurement of the state of a plant with parametric uncertainties

**Del-AR-P (Passive)** Simulation of a passive response to an anomaly which intro-

duces a time delay into the measurement of the state of a plant with parametric uncertainties, and the nominal adaptive autopilot retains control without intervention from the remote human supervisor

### 5.1.2 Actuator Fault Simulations

The first anomaly considered in simulation (**Act-AR**), corresponding to the problem stated in Section 2.1.1, is the abrupt occurrence of an actuator fault, which is assumed to change the actuator dynamics from a direct gain (2.3) to a first-order lag (2.4). By applying the change in dynamics defined in (2.4), and choosing  $T_l = 1.0\text{s}$ , the plant dynamics change from (5.7) to

$$\underbrace{\begin{bmatrix} \dot{\phi} \\ \dot{p} \\ \ddot{p} \end{bmatrix}}_{\dot{x}'_p} = \underbrace{\begin{bmatrix} 0 & 1 & 0 \\ 0 & 0 & 1 \\ 0 & -1.10 & -2.10 \end{bmatrix}}_{A'_p} \underbrace{\begin{bmatrix} \phi \\ p \\ \dot{p} \end{bmatrix}}_{x'_p} + \underbrace{\begin{bmatrix} 0 \\ 0 \\ 0.318 \end{bmatrix}}_{B'_p} u \quad (5.10)$$

at  $t = t_1^*$ , corresponding to the higher-order plant model given by (2.5). This results in the open-loop transfer function

$$\frac{\Phi(s)}{U(s)} = \frac{0.318}{s^3 + 2.10s^2 + 1.10s}. \quad (5.11)$$

Using this pilot input, we propose an adaptive controller predicated on a third-order dynamics of the open-loop plant and assume that in addition to the bank angle and roll rate, angular acceleration  $\dot{p}$  is also measurable. We choose a reference model as

$$\underbrace{\begin{bmatrix} \dot{\phi}_d \\ \dot{p}_d \\ \ddot{p}_d \end{bmatrix}}_{\dot{x}'_m} = \underbrace{\begin{bmatrix} 0 & 1 & 0 \\ 0 & 0 & 1 \\ -32 & -32 & -10 \end{bmatrix}}_{A'_m} \underbrace{\begin{bmatrix} \phi_d \\ p_d \\ \dot{p}_d \end{bmatrix}}_{x'_m} + \underbrace{\begin{bmatrix} 0 \\ 0 \\ 32 \end{bmatrix}}_{B'_m} r - \underbrace{\begin{bmatrix} -10 & -1 & 0 \\ 0 & -10 & -1 \\ 32 & 32 & 0 \end{bmatrix}}_{L'_m} e' \quad (5.12)$$

After detection and diagnosis of the anomaly with the shared decision-making

framework, involving Tasks 1–3 by the human as described in Section 3.2, the corrective action to increase the dimension of the controller is made at  $t = t_2^*$ , and the reference model dynamics is switched to that of (5.12). The control gains which will cause the closed-loop roll response to match the desired response exactly are

$$\theta^*(t) = \begin{cases} \begin{bmatrix} -25.16, & -15.41 \end{bmatrix} & t < t_1^* \\ \begin{bmatrix} -32.00, & -30.90, & -2.10 \end{bmatrix} & t \geq t_1^* \end{cases} \quad (5.13)$$

$$q^*(t) = \begin{cases} 25.16 & t < t_1^* \\ 32.00 & t \geq t_1^* \end{cases} \quad (5.14)$$

which are unknown to the adaptive controller. As mentioned earlier, initial values are chosen as  $\theta(t = 0) = [-25.16, -15.41]$  and  $q(t = 0) = 25.16$ . The learning rates in (3.9) and (3.10) were chosen to be  $\Gamma_\theta = 10I_2$ , with  $I_n$  the identity matrix of dimension  $n$ , and  $\gamma_q = 10$ . The projection operator was not used in this simulation. It was assumed that  $t_1^* = 30\text{s}$  and  $t_2^* = 90\text{s}$ . To add more realism to the simulation example, we have assumed that the signal  $\dot{p}$  is not directly measured, and instead use a high-pass filter to estimate it from  $p$  using  $\hat{p} = \frac{as}{s+a}p$ . Results of this simulation are given in Figures 5-1, 5-2, 5-3, and 5-4.

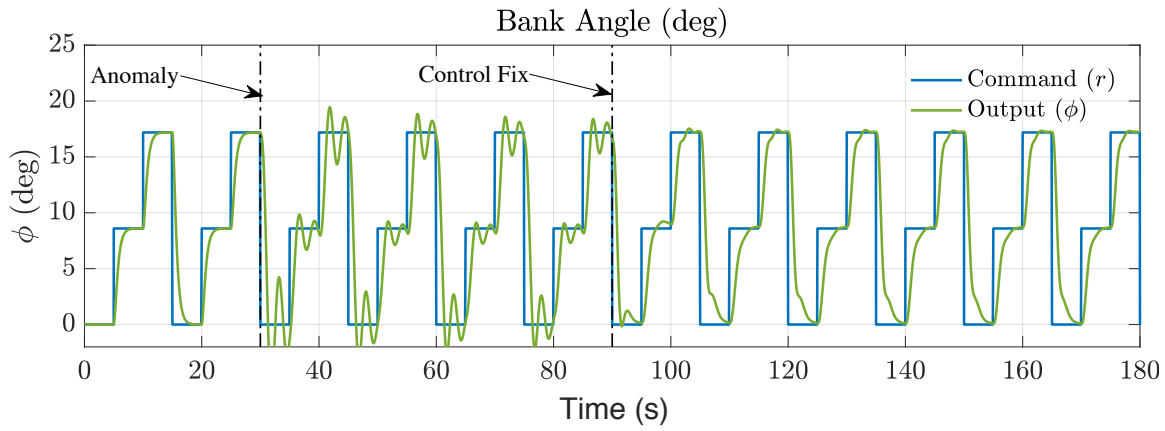


Figure 5-1: Act-AR simulation: Bank angle command ( $r(t)$ ) and output ( $\phi(t)$ ) in nominal operation ( $t \leq t_1^*$ ), after change in actuator dynamics ( $t_1^* < t \leq t_2^*$ ), and after a corrective action ( $t > t_2^*$ )

From Figures 5-1, 5-2, and 5-3, it is clear that after an initial adaptation period,

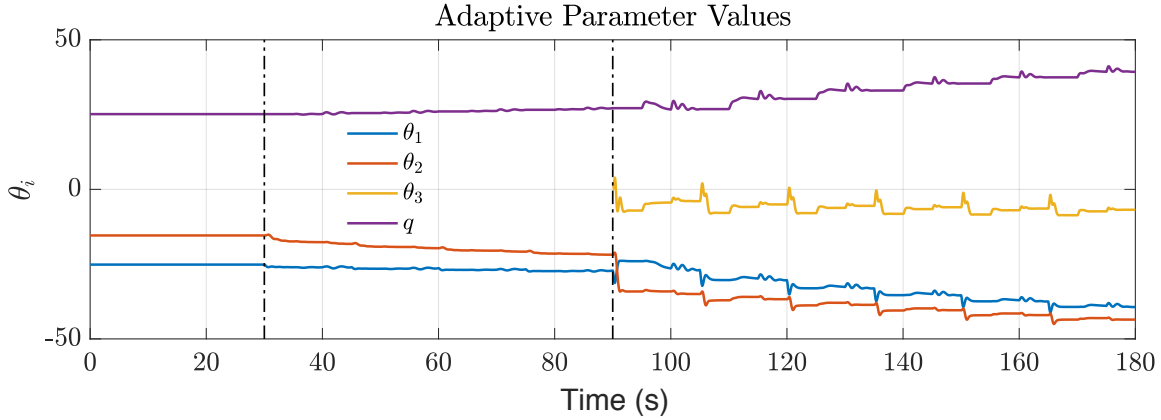


Figure 5-2: Act-AR simulation: Adaptive feedback gains in nominal operation ( $t \leq t_1^*$ ), after change in actuator dynamics ( $t_1^* < t \leq t_2^*$ ), and after a corrective action ( $t > t_2^*$ )

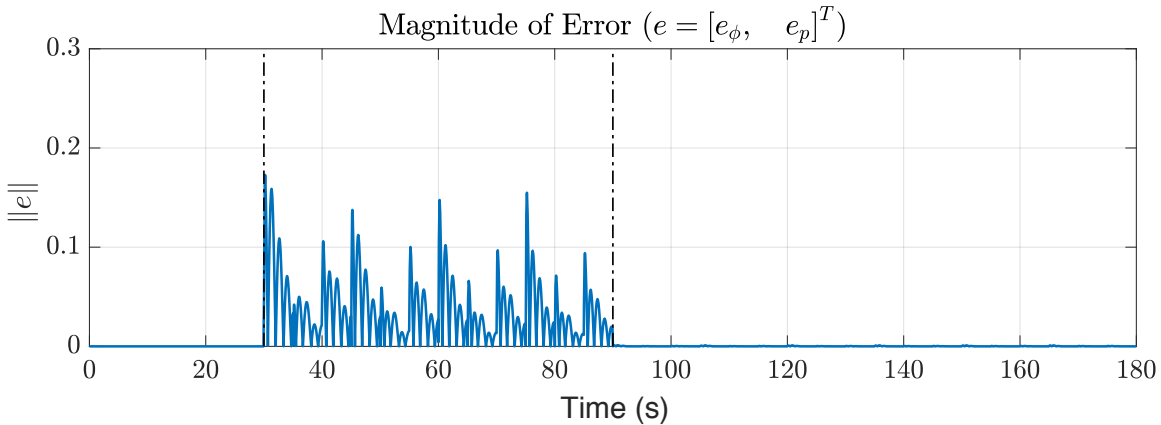


Figure 5-3: Act-AR simulation: Tracking error  $\|e(t)\|$  in nominal operation ( $t \leq t_1^*$ ), after change in actuator dynamics ( $t_1^* < t \leq t_2^*$ ), and after a corrective action ( $t > t_2^*$ )

the adaptive controller with third-order reference model dynamics converges on the desired feedback/feedforward gains, returning the roll control to its satisfactory performance without requiring any manual control from the human pilot. The action required from the human pilot is in the detection and diagnosis of the anomaly in dynamical behavior, leading to the addition of feedback on  $\hat{p}$  as a corrective action.

Analyses can be carried out on the simulation of the adaptive system by defining

average adaptive parameter values over time period  $(\mathcal{T} - \Delta t, \mathcal{T})$  as

$$\bar{\theta}(t = \mathcal{T}) = \frac{1}{\Delta t} \int_{\mathcal{T} - \Delta t}^{\mathcal{T}} \theta(t) dt \quad (5.15)$$

$$\bar{q}(t = \mathcal{T}) = \frac{1}{\Delta t} \int_{t_{f,i}\mathcal{T} - \Delta t}^{\mathcal{T}} q(t) dt. \quad (5.16)$$

Setting  $\Delta t = 5$ s and  $\mathcal{T} \in (t_1^*, t_2^*, t_{\text{sim}})$  permits the definition of a closed-loop frequency response which is representative of controller performance after parameter adaptation in each stage. Figure 5-4 shows the closed-loop unit step input responses with  $\bar{\theta}(\mathcal{T})$  and  $\bar{q}(\mathcal{T})$  for  $\mathcal{T} \in (t_2^* = 90, t_{\text{sim}} = 180)$ s, plotted alongside the ideal response with the nominal and recovery adaptive autopilots (the second- and third-order reference models, respectively), demonstrating how the characteristics of nominal operation are recovered with the adaptive controller with three feedback parameters.

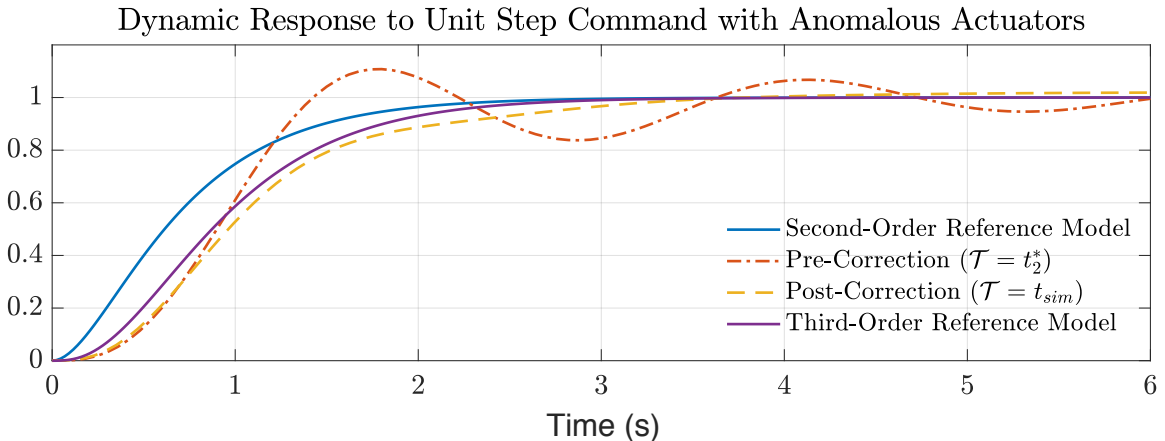


Figure 5-4: Act-AR analysis: Unit step responses for closed-loop transfer functions at different stages of simulation, demonstrating performance improvement after corrective action

### 5.1.3 Sensor Latency Simulations

The second type of anomaly considered in simulations (**Del-AR** and **Del-AR-P**), corresponding to the problem stated in Section 2.1.2, is the abrupt introduction of a time delay to sensor measurements. A time delay of  $\tau = 0.200$ s is added to the plant (5.2) between the state measurements and their use in control input computation as

in (2.7), so that

$$x_\sigma(t) = x_p(t - 0.20). \quad (5.17)$$

With  $\Phi_\sigma(s)$  defined as the delayed bank angle measurement, the change in the transfer function  $\Phi_\sigma(s)/U(s)$  is thus

$$\frac{\Phi_\sigma(s)}{U(s)} = \begin{cases} \frac{0.318}{s^2 + 1.10s} & t < t_1^* \\ \frac{0.318}{s^2 + 1.10s} e^{-0.20s} & t \geq t_1^* \end{cases} \quad (5.18)$$

For  $0 < t < t_1^*$ , the reference model used by the nominal adaptive controller in simulation is that given by (5.9). For  $t \geq t_1^*$ , the reference model used by the recovery adaptive controller in simulation is given by

$$\underbrace{\begin{bmatrix} \dot{\phi}_d \\ \dot{p}_d \\ \ddot{p}_d \end{bmatrix}}_{\dot{x}'_m} = \underbrace{\begin{bmatrix} 0 & 1 & 0 \\ 0 & 0 & 1 \\ -32 & -32 & -10 \end{bmatrix}}_{A'_m} \underbrace{\begin{bmatrix} \phi_d \\ p_d \\ \dot{p}_d \end{bmatrix}}_{x'_m} + \underbrace{\begin{bmatrix} 0 \\ 0 \\ 32 \end{bmatrix}}_{B'_m} r - \underbrace{\begin{bmatrix} -10 & -1 & 0 \\ 0 & -10 & -1 \\ 32 & 32 & 9.9 \end{bmatrix}}_{L'_m} e'. \quad (5.19)$$

Using the first-order delay approximation (2.9), given by

$$0.20\dot{x}_\sigma(t) + x_\sigma(t) = x_p(t), \quad (5.20)$$

the feedback and feedforward gains which would give the desired closed-loop response for  $\Phi_\sigma(s)/U(s)$  are

$$\theta^*(t) = \begin{cases} \begin{bmatrix} -25.16 & -15.41 \end{bmatrix} & t < t_1^* \\ \begin{bmatrix} -20.13 & -16.67 & -2.45 \end{bmatrix} & t \geq t_1^* \end{cases} \quad (5.21)$$

$$q^*(t) = \begin{cases} 25.16 & t < t_1^* \\ 20.13 & t \geq t_1^* \end{cases} \quad (5.22)$$

Parameter adaptation rates used in this simulation are given by

$$\Gamma_\theta = \begin{cases} 10I_2 & t < t_2^* \\ \text{diag}(10.0, 10.0, 0.1) & t \geq t_2^* \end{cases} \quad (5.23)$$

$$\gamma_q = 10.0 \quad \forall t \quad (5.24)$$

where the learning rate on  $\hat{p}$  is lower than that used in the simulation of an actuator fault, to improve robustness to the first-order approximation used to model the time delay. In addition, a projection operator with the following constant parameters (3.13) was used to limit  $\dot{\theta}(t)$

$$\varphi_m = [300, 200, 25] \quad (5.25)$$

$$\varphi_\epsilon = [50, 50, 25] \quad (5.26)$$

and the following constant parameters for the projection operator limiting  $\dot{q}(t)$

$$\varphi_m = 300 \quad (5.27)$$

$$\varphi_\epsilon = 50 \quad (5.28)$$

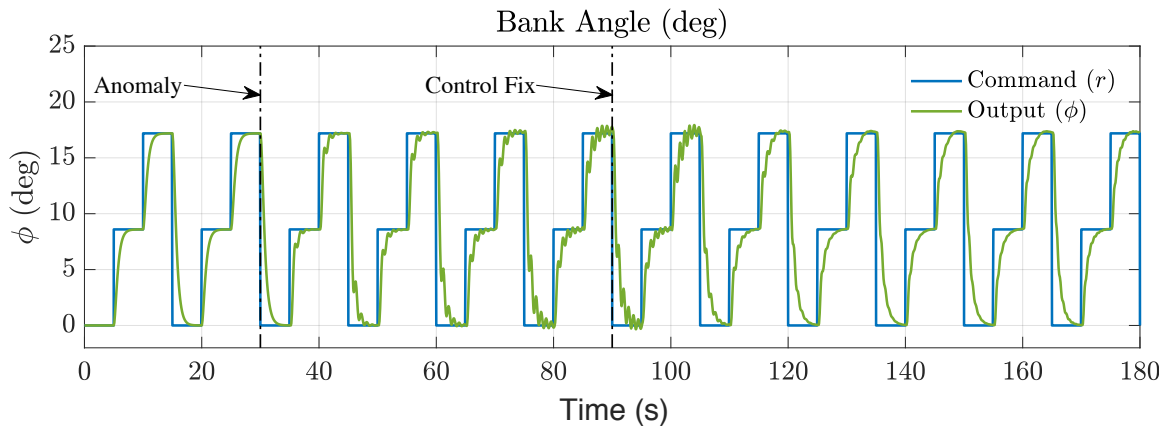


Figure 5-5: Del-AR simulation: Bank angle command ( $r(t)$ ) and output ( $\phi(t)$ ) in nominal operation ( $t \leq t_1^*$ ), after abrupt addition of a time delay ( $t_1^* < t \leq t_2^*$ ), and after a corrective action ( $t > t_2^*$ )

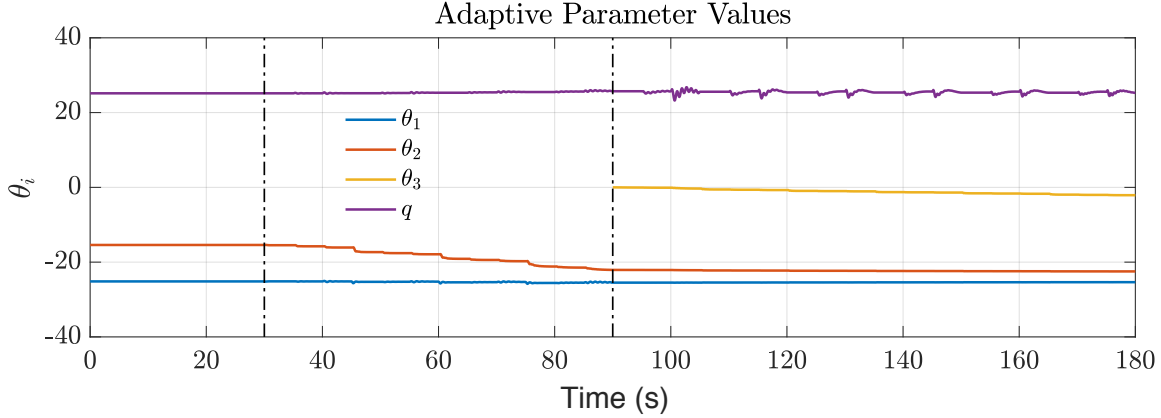


Figure 5-6: Del-AR simulation: Adaptive feedback gains in nominal operation ( $t \leq t_1^*$ ), after abrupt addition of a time delay ( $t_1^* < t \leq t_2^*$ ), and after a corrective action ( $t > t_2^*$ )

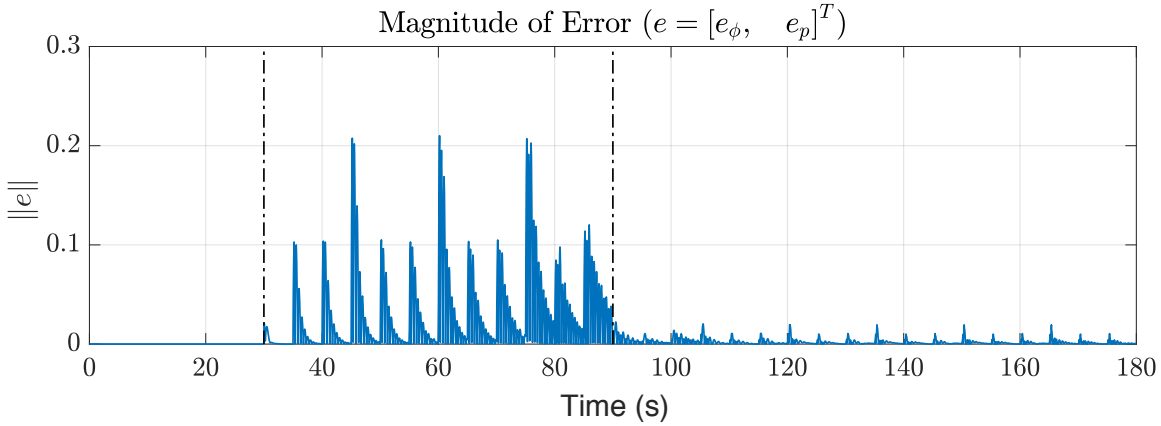


Figure 5-7: Del-AR simulation: Tracking error  $\|e(t)\|$  in nominal operation ( $t \leq t_1^*$ ), after abrupt addition of a time delay ( $t_1^* < t \leq t_2^*$ ), and after a corrective action ( $t > t_2^*$ )

The resulting responses of the shared controller are shown in Figures 5-5, 5-6, and 5-7. From these results, we see that the adaptive controller with two feedback parameters has trouble tracking the commanded bank angle after the introduction of an anomaly, but the addition of a third feedback parameter ( $\hat{p}$ ) and a corresponding increase in the dimension of the reference model allows the controller to recover a reasonable tracking performance. It is worth noting that the model-following error does not converge to zero even with the recovery adaptive controller given by (3.1), (3.9), (3.10), and (5.12), because of the approximation of the latency in the model as a first-order lag.

The transfer functions used to generate step response plots in Figure 5-8 use (5.15) and (5.16) for average parameter values. Although the step response characteristics of the system following the switch to recovery adaptive controller ( $\mathcal{T} = t_{\text{sim}}$ ) differ more from nominal operation compared to the case of a change in actuator dynamics (in Figure 5-4), it is significantly more satisfactory than the closed-loop response before the correction ( $\mathcal{T} = t_2^*$ ).

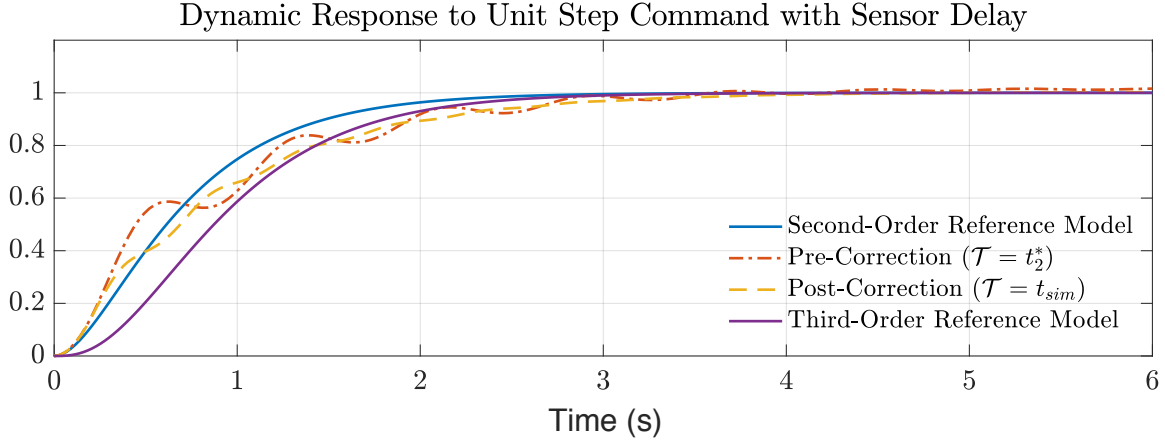


Figure 5-8: Del-AR analysis: Unit step responses for closed-loop transfer functions at different stages of simulation, demonstrating performance improvement after corrective action

This successful shared control response to an anomaly which introduced latency into sensor measurements (Del-AR) contrasts sharply with a passive response (Del-AR-P), in which the human pilot takes no action. In this case, the nominal adaptive controller retains responsibility for command tracking and regulation, which leads to structural failure at  $t_3^* = 107$ s. Command tracking, and eventual failure in a simulation of this passive response is displayed in Figure 5-9. It is noted that a shared control response with  $t_2^* < t_3^*$  will lead to recovery of closed-loop tracking performance.

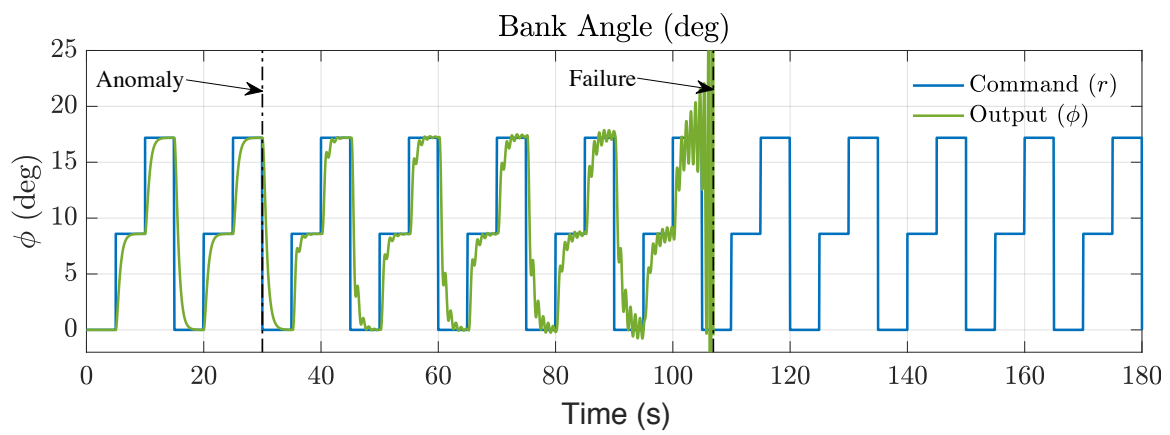


Figure 5-9: Del-AR-P simulation (passive anomaly response): The vehicle loses closed-loop stability following the anomaly when the shared control response is not implemented, and failure occurs at  $t = t_3^*$

## 5.2 MIMO Output Feedback and Remote Pilot

The shared control solution introduced in Chapter 4 is applied to the problem introduced in Section 2.2 on a high altitude, long endurance (HALE) flexible aircraft model. HALE aerial platforms, such as the solar-electric NASA/AeroVironment Helios and Facebook Aquila, have unique design considerations to satisfy goals of uninterrupted weeks- or months-long operation. To reduce power draw, HALE aircraft designs save mass by allowing wings to bend, and may be classified as very flexible aircraft (VFA) [7]. Compared to typical fixed-wing aircraft, these aircraft operate at low speed, and may use low-bandwidth actuators which must be accounted for in control design. HALE VFA platforms are likely to have significant modeling uncertainties and online variation in dynamics due to flexible effects and degradation over long-term operation. It is assumed that these vehicles are unmanned and that they require supervision from remote human operators as needed.

The aircraft model used in simulation, developed in Ref. [7] for longitudinal control design applications, is rendered in Figure 5-10 and described in Section 5.2.1. The results of numerical simulations on the control and anomaly recovery with this MIMO plant are then presented in Section 5.2.2, comparing the shared anomaly response to alternative anomaly responses.

### 5.2.1 HALE Aircraft Longitudinal Dynamics

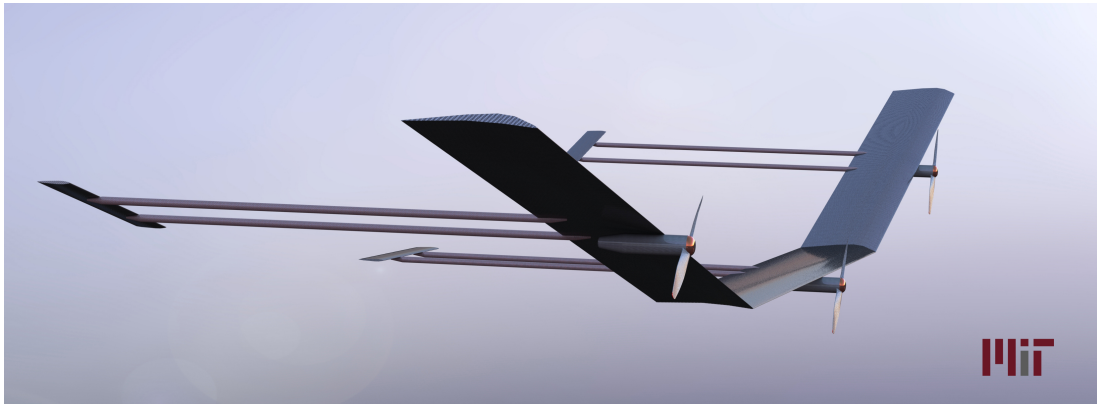


Figure 5-10: Rendering of very flexible aircraft model used in numerical simulations

The aircraft model represents the nonlinear longitudinal dynamics of a highly flexible HALE UAV concept with three rigid lifting sections, hinged together such that the aircraft is able to bend at the joints of the three sections. The pitch mode dynamics of this nonlinear model is defined using the state vector

$$x_{\text{vfa}} = \begin{bmatrix} V \\ \alpha \\ h \\ \theta \\ q \\ \eta \\ \dot{\eta} \end{bmatrix} = \begin{bmatrix} \text{Airspeed (ft/s)} \\ \text{Angle of attack (rad)} \\ \text{Altitude (ft)} \\ \text{Pitch angle (rad)} \\ \text{Pitch rate (rad/s)} \\ \text{Dihedral (rad)} \\ \text{Dihedral rate (rad/s)} \end{bmatrix}. \quad (5.29)$$

We linearize and trim the aircraft in straight and level flight using the inputs

$$u_{\text{vfa}} = \begin{bmatrix} \delta_{th} \\ \delta_{a,c} \\ \delta_{a,o} \\ \delta_{e,c} \\ \delta_{e,o} \end{bmatrix} = \begin{bmatrix} \text{Thrust (lbf)} \\ \text{Center aileron (rad)} \\ \text{Outer aileron (rad)} \\ \text{Center elevator (rad)} \\ \text{Outer elevator (rad)} \end{bmatrix}. \quad (5.30)$$

Assuming small deviations in altitude, the state vector can be reduced to

$$x_p = [V \quad \alpha \quad \theta \quad q \quad \eta \quad \dot{\eta}]^T \quad (5.31)$$

which corresponds to the state of the plant in (2.11). We consider the control task of tracking commands for the dihedral angle and vertical acceleration, using control inputs  $\delta_{a,o}$  and  $\delta_{e,c}$  only, so the vector  $u_p$  in (2.11) is

$$u_p = [\delta_{a,o} \quad \delta_{e,c}]^T. \quad (5.32)$$

Regulation of the dihedral angle is desired, as a large dihedral angle is inefficient

for lift generation and introduces instability in the open-loop dynamics, while a small dihedral angle will require more control effort to hold, increasing drag and power requirements and imparting twisting moments on the aircraft.

The measurements available for control design are the pitch rate, dihedral angle, and vertical acceleration, leading to plant outputs

$$\begin{aligned} y_p &= \begin{bmatrix} q \\ \eta \\ A_z \end{bmatrix} = \begin{bmatrix} \text{Pitch rate (rad/s)} \\ \text{Dihedral angle (rad)} \\ \text{Vertical acceleration (ft/s)} \end{bmatrix} \\ z_p &= \begin{bmatrix} \eta \\ A_z \end{bmatrix} = \begin{bmatrix} \text{Dihedral angle (rad)} \\ \text{Vertical acceleration (ft/s)} \end{bmatrix} \end{aligned} \quad (5.33)$$

and the outputs for the augmented plant (4.2),

$$y = \begin{bmatrix} q \\ \int z_p - z_{cmd} \end{bmatrix}, \quad z = z_p. \quad (5.34)$$

For numerical simulations, the VFA model is trimmed at an airspeed of 68 ft/s, altitude of 40,000 ft, 2.8° angle of attack and pitch angle (level flight), and dihedral angles ranging from 0° to 20° in 1° increments. Figure 5-11 shows pole locations of the linearized plant for different dihedral angles, and Figure 5-12 shows instability of the linearized plant when trimmed above 11° dihedral. Figure 5-13 shows the thrust and control surface deflections for the trimmed VFA model over a range of dihedral angles.

The plant is augmented with a linear actuator model corresponding to (2.12) in the nominal case and (2.13) in the presence of anomalous dynamics. The vehicle simulation with first-order actuators (2.12) uses time constants  $(\hat{\tau}, \tau) = (0.5, 2.0)$ s in the control model and the actual plant, respectively, corresponding to

$$D_1 = 2I_2, \quad \Theta_1 = -1.5I_2 \quad (5.35)$$

where  $\Theta_1$  is unknown for control design, and  $I_2$  is the  $2 \times 2$  identity matrix.

Simulation of the anomalous dynamics (2.13) uses second-order actuators with

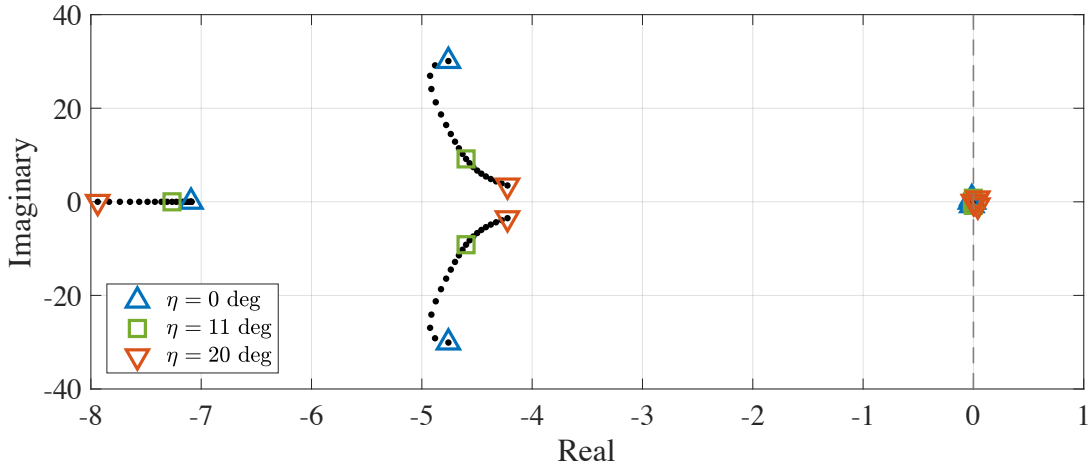


Figure 5-11: Poles of linearized open-loop HALE VFA dynamics for different dihedral angles, in the complex plane

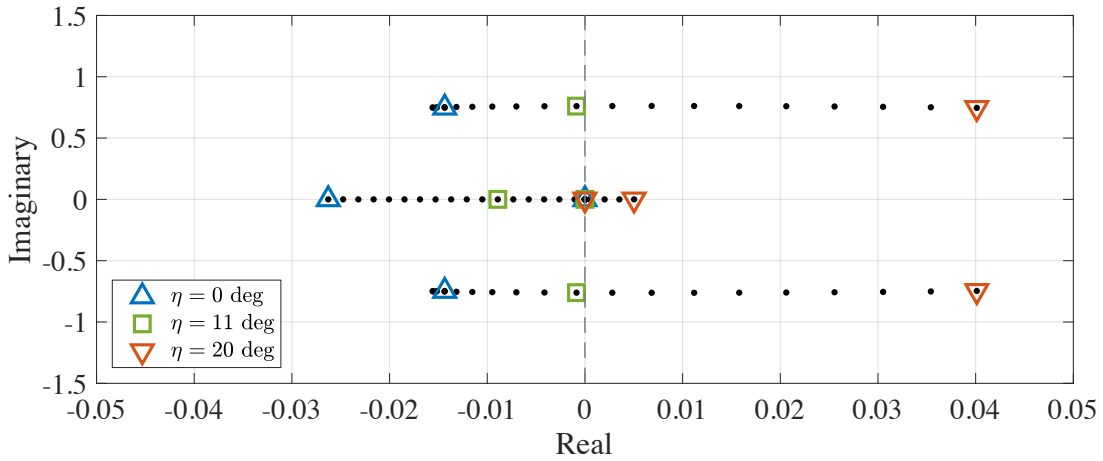


Figure 5-12: Dominant poles of linearized open-loop HALE VFA dynamics, which move into the right-half complex plane when  $\eta > 11^\circ$

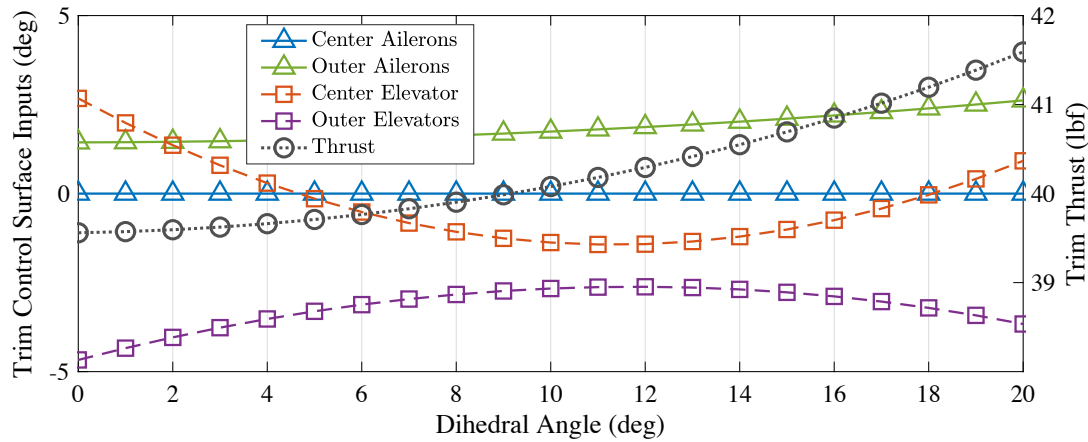


Figure 5-13: Actuator trim at different dihedral angles

cutoff frequencies  $(\hat{\omega}_c, \omega_c) = (2.0, 1.0)$  rad/s and damping ratios  $(\hat{\zeta}, \zeta) = (0.7, 0.8)$  in the control model and actual plant, respectively, corresponding to

$$\begin{bmatrix} D_1 \\ D_2 \end{bmatrix} = \begin{bmatrix} 4I_2 \\ 2.8I_2 \end{bmatrix}, \quad \begin{bmatrix} \Theta_1 \\ \Theta_2 \end{bmatrix} = \begin{bmatrix} -3.75I_2 \\ -2I_2 \end{bmatrix} \quad (5.36)$$

where  $\Theta_1$  and  $\Theta_2$  are unknown for control design. Matrices  $\Theta_p$  and  $\Lambda_p$  used in simulation represent modeling errors that are assumed to be caused by linearization of the VFA model at an incorrect dihedral angle, and an 80% reduction in actuator effectiveness, respectively, and are given by

$$\Theta_p^T = \begin{bmatrix} 0.6 & -4.52 & 0 & 0.05 & 0.41 & 1.47 \\ 0.1 & 1.83 & 0 & -0.02 & -0.35 & -0.59 \end{bmatrix} \quad (5.37)$$

$$\Lambda = 0.2I_2.$$

Both the nominal and recovery adaptive controllers utilize a number of free design parameters, including LQR weight matrices and adaptation rates. These parameters are tabulated in Appendix A.

### 5.2.2 Simulations

We begin by simulating the HALE VFA under nominal autonomous control, responding to step inputs in commands for the dihedral angle and vertical acceleration, with the following three variants.

**Nom-1** Command tracking using baseline RSLQR controller without uncertainty  
 $(\Theta_p = 0, \Lambda_p = 0, \Theta_1 = 0)$

**Nom-2** Command tracking using baseline RSLQR controller with uncertainty ( $\Theta_1$  in (5.35);  $\Theta_p, \Lambda_p$  in (5.37))

**Nom-3** Command tracking using [baseline RSLQR + adaptive] controller with uncertainty ( $\Theta_1$  in (5.35);  $\Theta_p, \Lambda_p$  in (5.37))

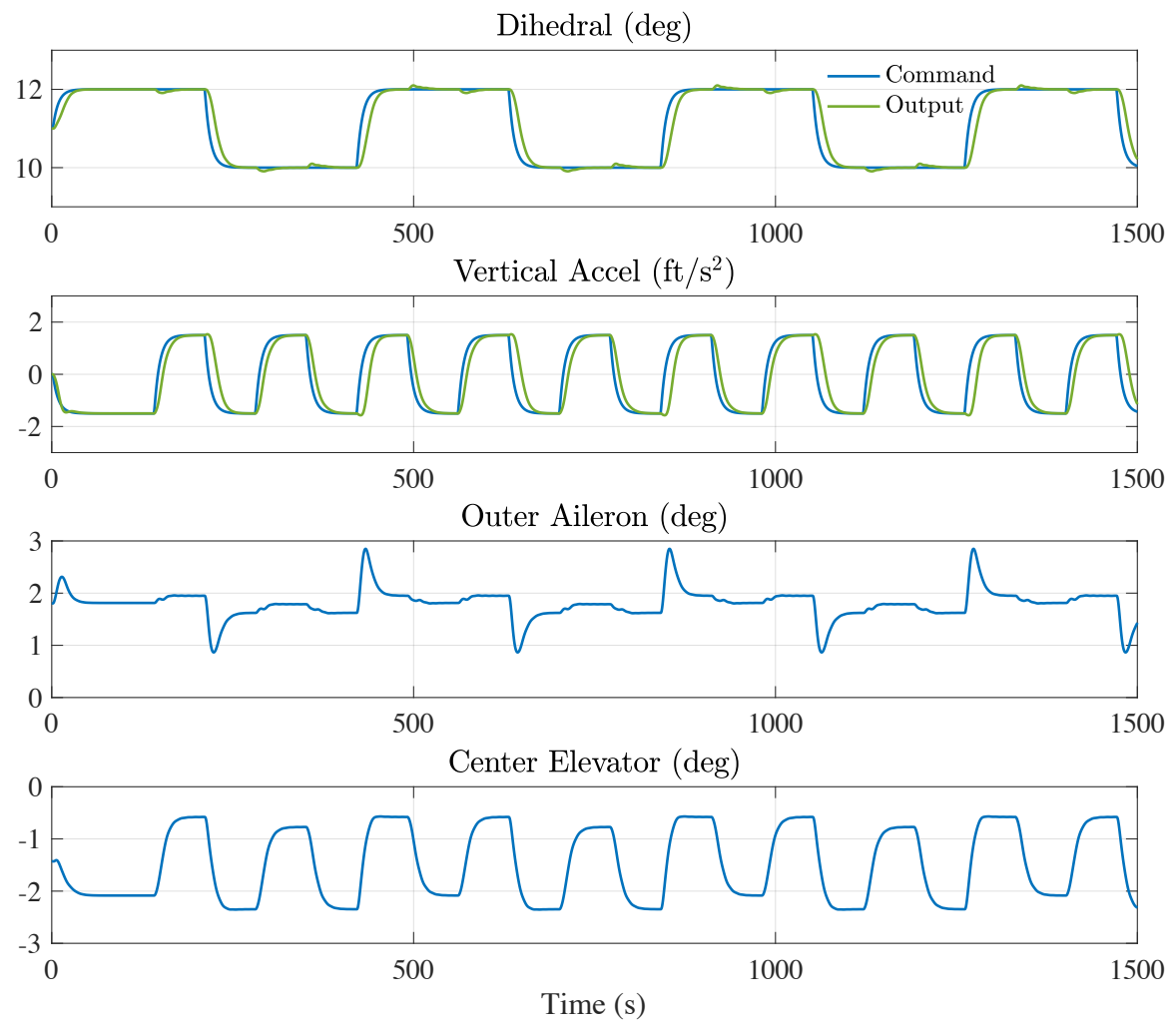


Figure 5-14: Nom-1 simulation: Control of longitudinal dynamics of VFA model using RSLQR, with no uncertainty in the control model

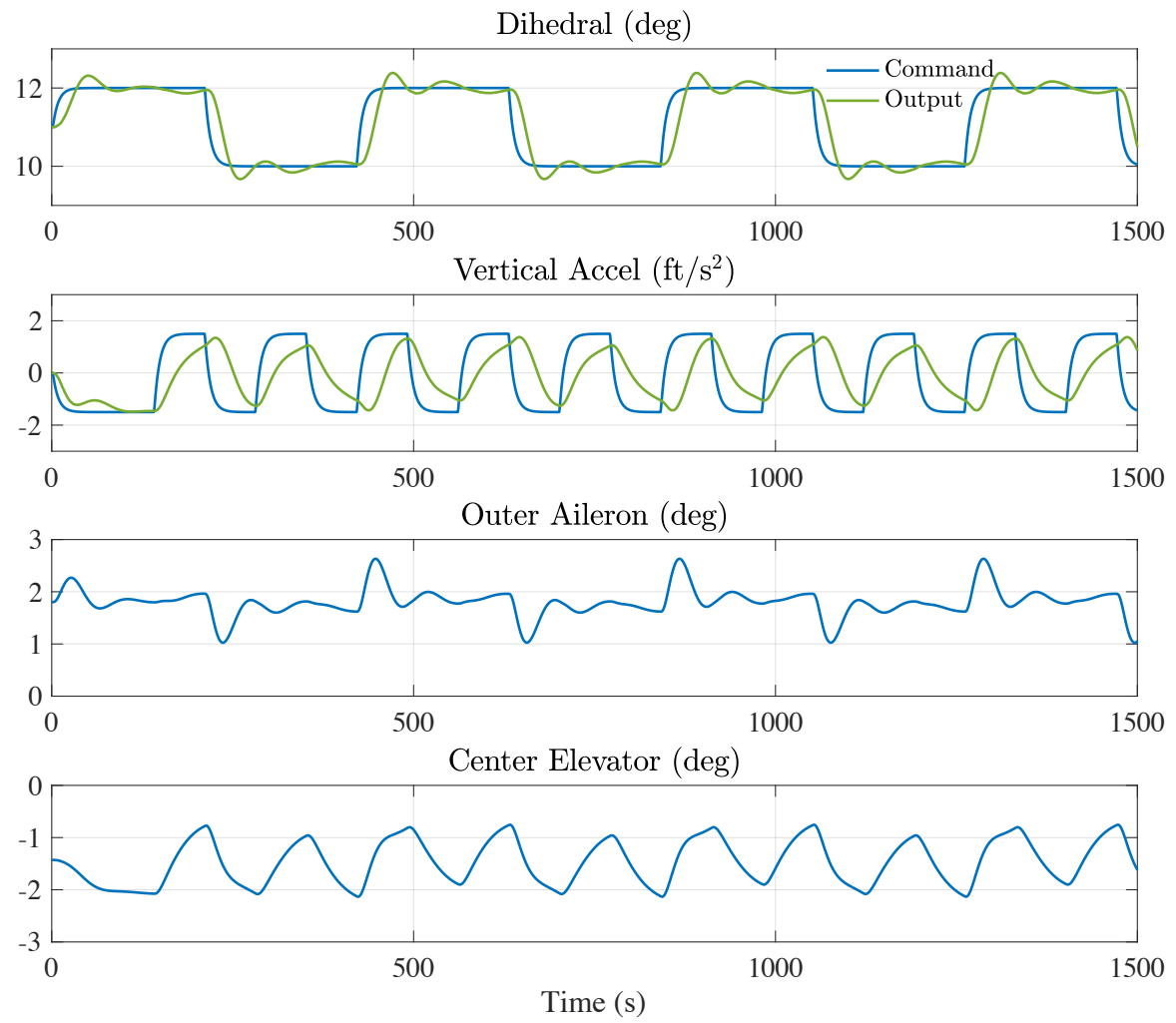


Figure 5-15: Nom-2 simulation: Control of longitudinal dynamics of VFA model using RSLQR, with uncertainties  $\Theta_p$ ,  $\Lambda_p$ , and  $\Theta_1$

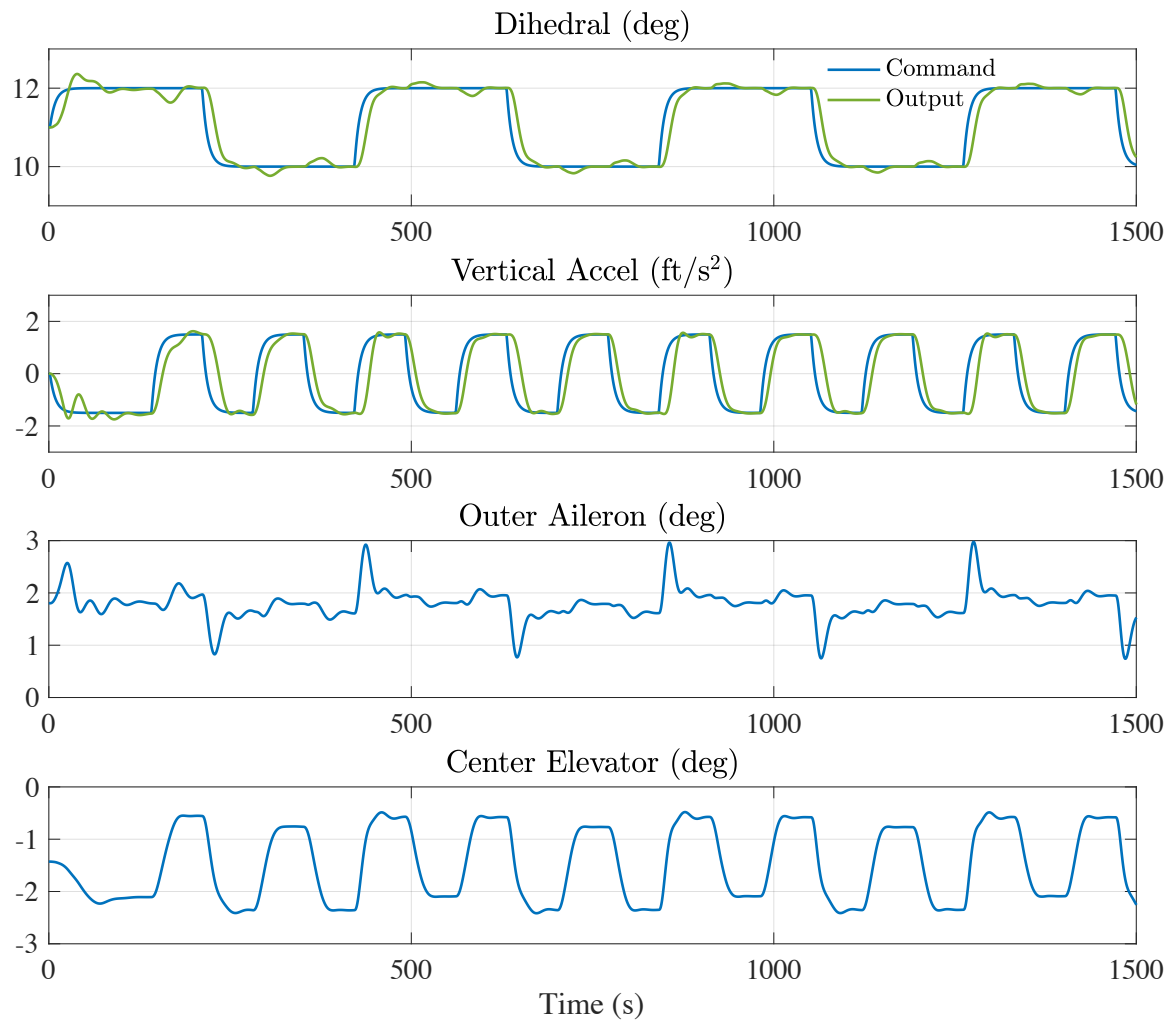


Figure 5-16: Nom-3 simulation: Control of longitudinal dynamics of VFA model using RSLQR + adaptive control, with uncertainties  $\Theta_p$ ,  $\Lambda_p$ , and  $\Theta_1$

These simulations, presented in Figures 5-14, 5-15, and 5-16 respectively, show how the adaptive controller with output feedback described in (4.5)–(4.17) is able to recover the desired closed-loop performance with uncertainty in plant and actuator parameters. With the baseline RSLQR controller only, the system suffers degraded command tracking performance in the presence of uncertainty (Figure 5-15), especially for vertical acceleration tracking.

In what follows, we simulate the introduction of an anomaly into the dynamics, causing the vehicle’s actuators to change abruptly from the uncertain first-order dynamics (2.12) to the uncertain second-order dynamics (2.13) at  $t_1^* = 600s$ . We consider three responses to the anomaly.

**AR-1 (Passive)** The nominal adaptive autopilot retains control without intervention from the remote human supervisor

**AR-2 (Manual)** The remote human operator takes over manual control of the affected vehicle

**AR-3 (Shared)** Responsibilities are shared between the human pilot and autopilot as described in Chapter 4

In these simulations, the vehicle operates in nominal operation with the [RSLQR + adaptive] control design for  $0 \leq t < t_1^*$ . At  $t_1^* = 600s$ , the vehicle’s actuators change from first-order (2.12) to second-order (2.13). Figures 5-17 to 5-19 show the result of a passive response (AR-1) in which the human operator ignores vehicle performance degradation and allows the adaptive controller to continue operating on the plant with severely anomalous dynamics. The closed-loop system loses stability, leading to oscillations in vehicle output and eventual structural failure of the VFA at  $t_3^* = 960s$ , 6 minutes after the introduction of second-order actuator dynamics. It is worth noting the rapid increase in magnitude of the adaptive parameters and the magnitudes of both tracking and measurement output error signals after the introduction of anomalous dynamics. For comparison to a baseline without adaptive control, a passive response using only the RSLQR controller (denoted AR-1-LQR)

leads to structural failure following the anomaly, at  $t = 1240s$ , as shown in Figure 5-20.

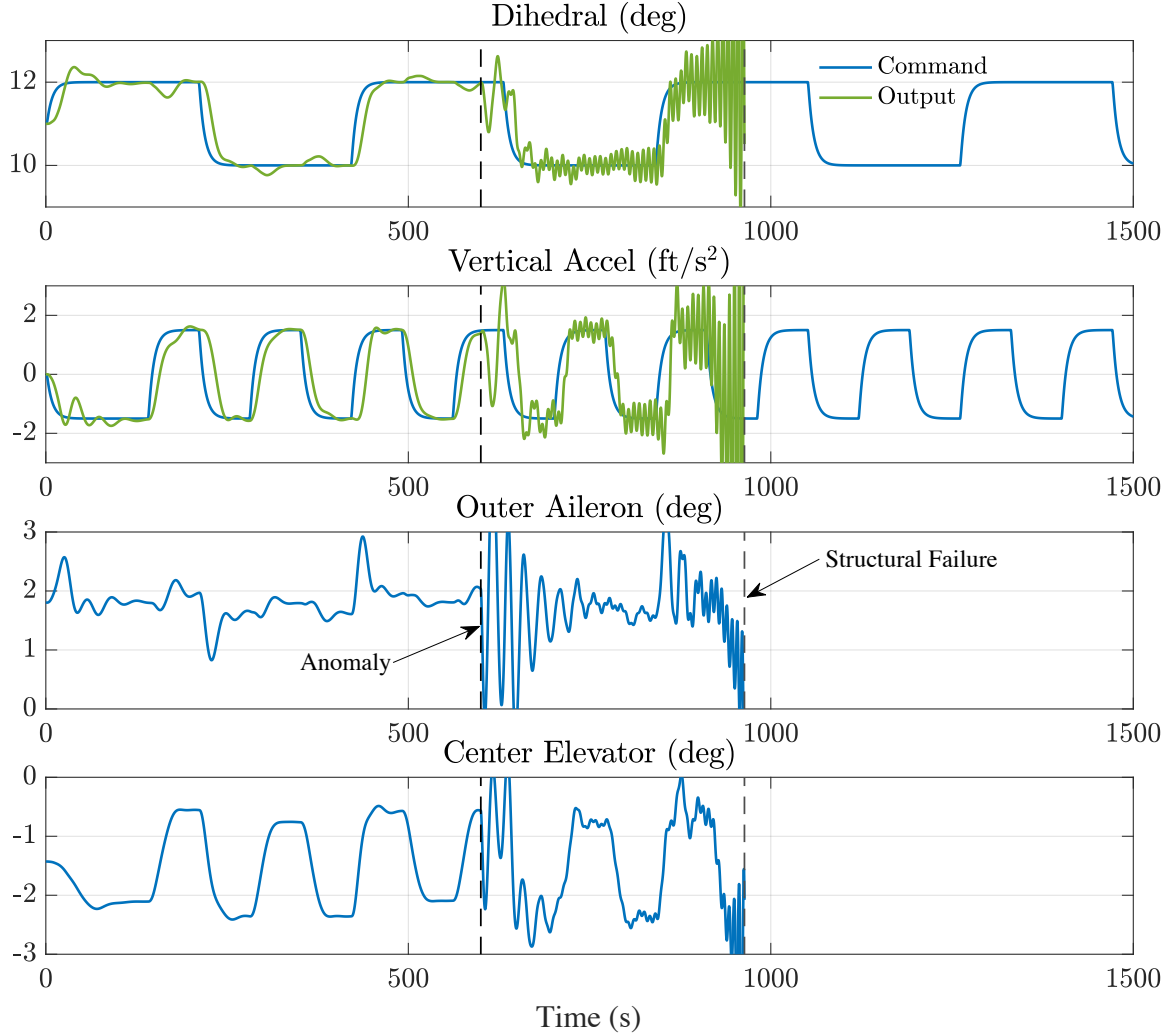


Figure 5-17: AR-1 simulation: Passive response to dynamical anomaly results in structural failure after 6 minutes

Numerical simulations of the AR-2 response (purely manual control) are not carried out here, as they are not deterministic and require high-fidelity *human-in-the-loop* experiments to characterize. The limitations of such a response – in which the human operator’s role changes suddenly from “on-the-loop” to “in-the-loop” with unfamiliar dynamics – are discussed in the earlier sections of this thesis, and in references elsewhere (e.g. [5], [13]).

Results of the AR-3 (shared control) anomaly response simulation are shown in

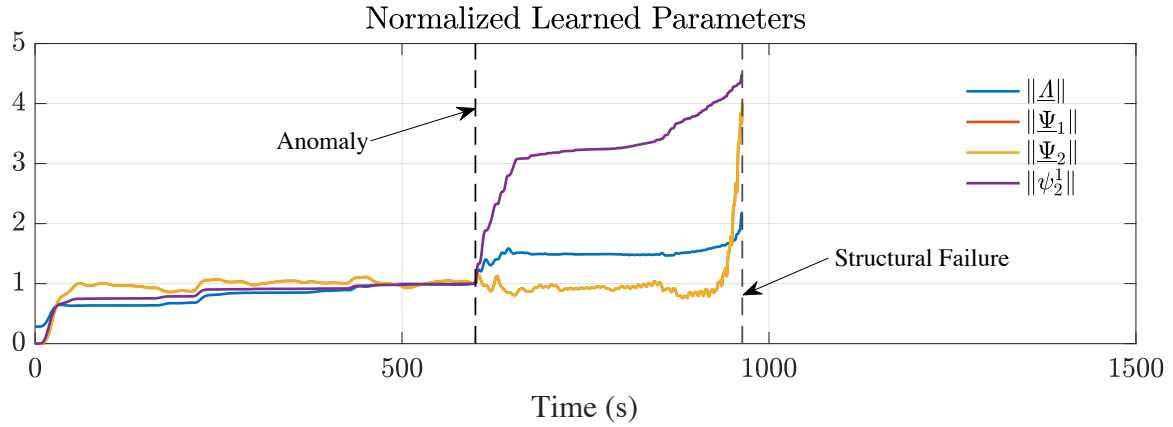


Figure 5-18: AR-1 simulation: Adaptive parameters diverge as controller struggles to adapt to unmodeled dynamics

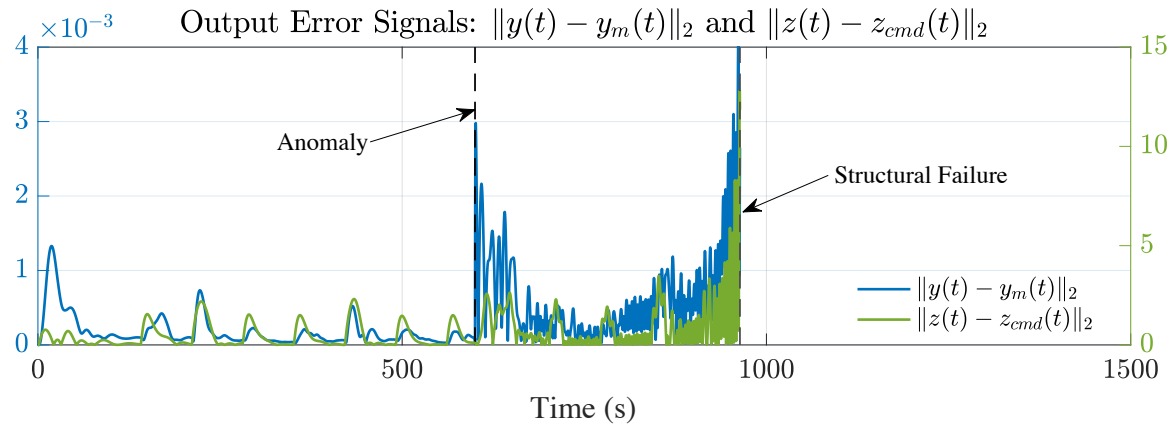


Figure 5-19: AR-1 simulation: Model-following output error and command tracking error grow due to anomalous dynamics

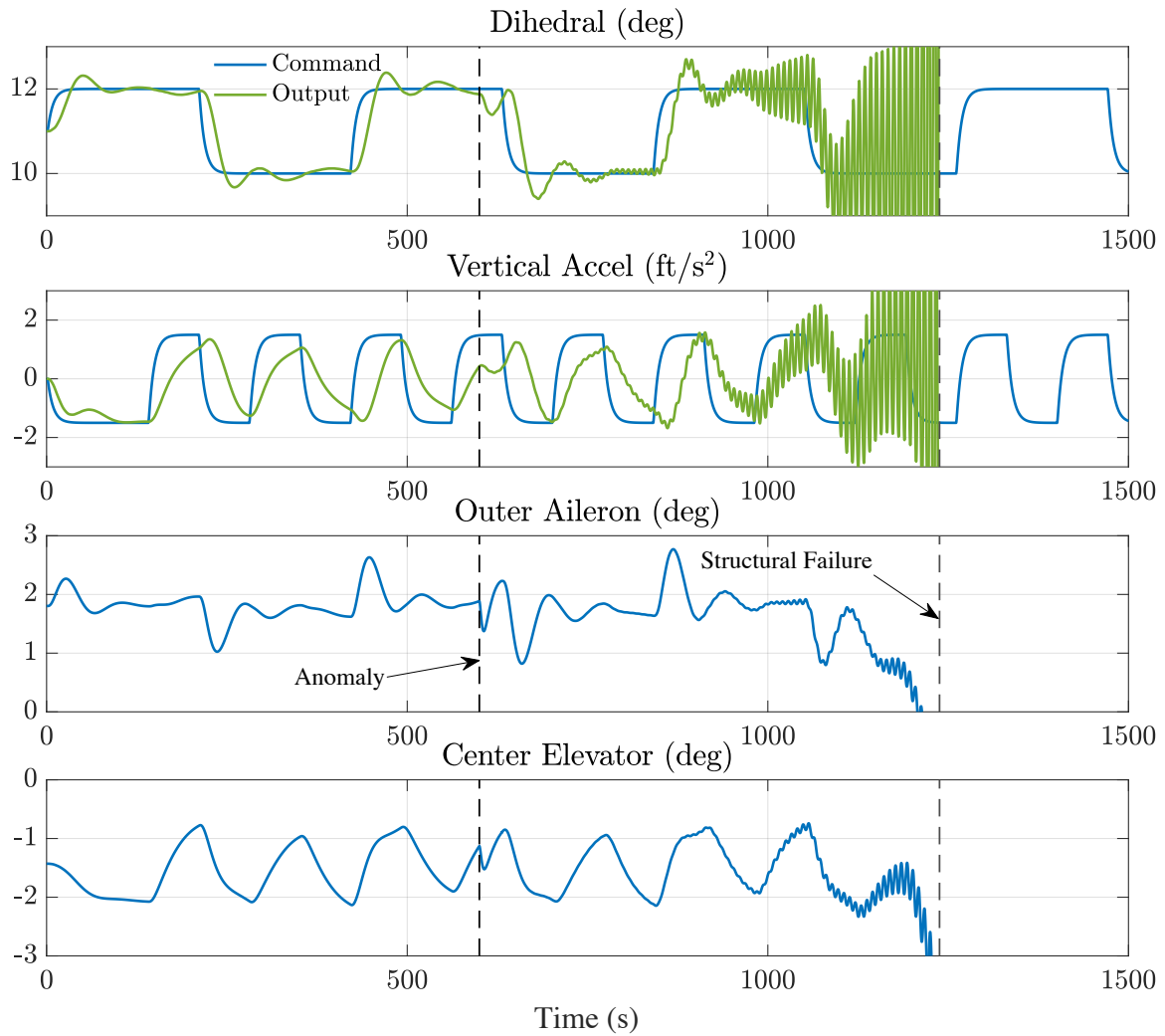


Figure 5-20: AR-1-LQR simulation: Passive response to dynamical anomaly using only baseline RSLQR control (no adaptive) also results in structural failure

Figures 5-21 to 5-23. After the anomaly is introduced at  $t_1^* = 600s$ , the nominal adaptive controller attempts to control the system whose dynamics are not fully accounted for in the control model. Simultaneously in the shared control framework, the human operator notices the anomalous closed-loop control behavior, and via an interface switches the controller to the higher relative degree design (4.19)–(4.38) at  $t_2^* = 800s$ , which is the culmination of the human operator’s action. For  $t \geq t_2^*$ , the vehicle remains under autonomous control with the recovery adaptive controller and is able to reestablish nominal command tracking performance and avert failure (which was assumed to occur at  $t_3^* = 960s$  with AR-1).

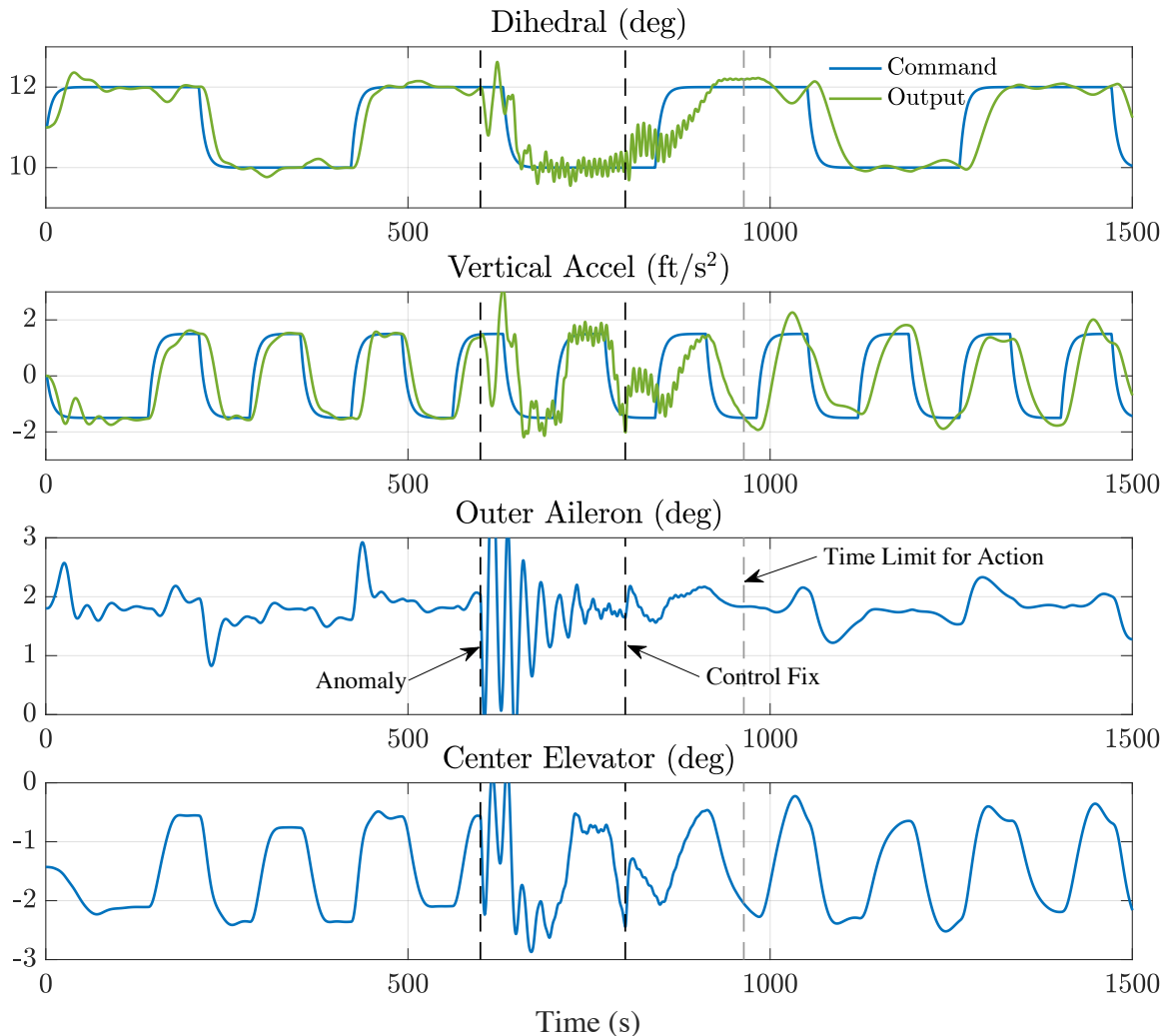


Figure 5-21: AR-3 simulation: Shared response to the dynamical anomaly results in recovery of vehicle performance

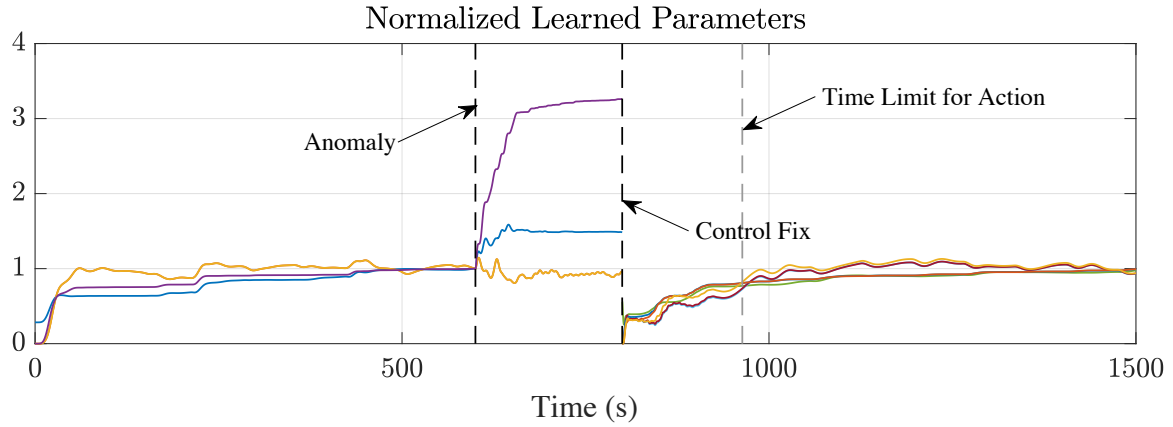


Figure 5-22: AR-3 simulation: The change in control model at  $t_2^* = 800s$  stops the divergence of adaptive parameters

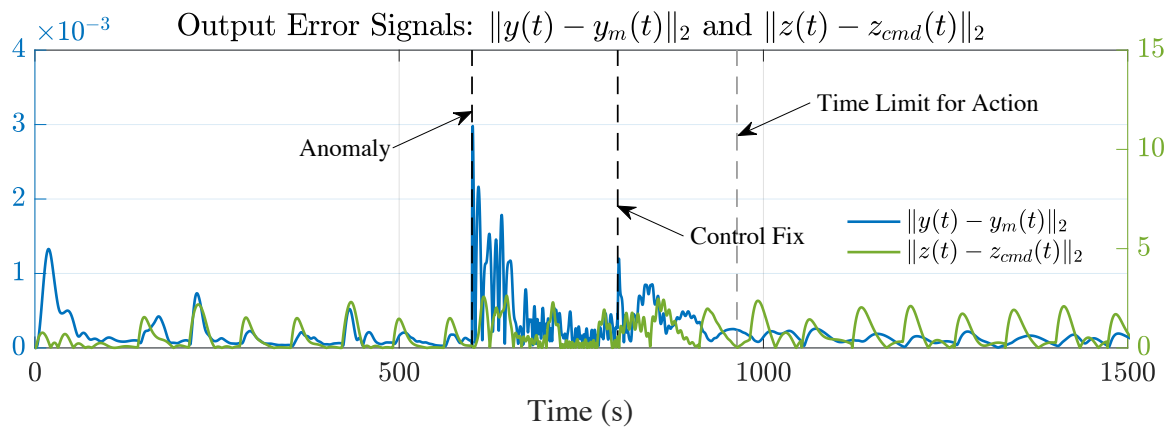


Figure 5-23: AR-3 simulation: The change in control model at  $t_2^* = 800s$  stops the error growth seen after the anomaly

Simulation	Dynamics Model	$t_1^*$	$t_2^*$	$t_3^*$	$t_{\text{sim}}$
<b>Act-AR:</b> shared control response to actuator lag anomaly	B747 Roll Mode	30 s	90 s	N/A	180 s
<b>Del-AR:</b> shared control response to sensor delay anomaly	B747 Roll Mode	30 s	90 s	N/A	180 s
<b>Del-AR-P:</b> passive response to sensor delay anomaly	B747 Roll Mode	30 s	N/A	107 s	180 s
<b>Nom-1:</b> nominal VFA command tracking without uncertainty	VFA Pitch Mode	N/A	N/A	N/A	1500 s
<b>Nom-2:</b> baseline (RSLQR) VFA command tracking with uncertainty	VFA Pitch Mode	N/A	N/A	N/A	1500 s
<b>Nom-3:</b> adaptive VFA command tracking with uncertainty	VFA Pitch Mode	N/A	N/A	N/A	1500 s
<b>AR-1:</b> adaptive VFA command tracking with uncertainty and actuator lag anomaly	VFA Pitch Mode	600 s	N/A	960 s	1500 s
<b>AR-1-LQR:</b> baseline (RSLQR) VFA command tracking with uncertainty and actuator lag anomaly	VFA Pitch Mode	600 s	N/A	1240 s	1500 s
<b>AR-3:</b> shared control response to actuator lag anomaly	VFA Pitch Mode	600 s	800 s	N/A	1500 s

Table 5.1: Summary of the simulations presented in Chapter 5.  $t_1^*$  denotes the time of anomaly occurrence,  $t_2^*$  denotes the time of the human completing anomaly response tasks,  $t_3^*$  denotes the time of plant/controller failure,  $t_{\text{sim}}$  denotes the simulation length.

# Chapter 6

## Concluding Remarks

This thesis developed a shared control architecture which synthesizes the actions of adaptive autopilots and human operators of aerial vehicles. Humans faced with the control of plants having unfamiliar dynamics attempt to adapt their control strategies, but their performance deteriorates while the risk of loss of control increases. Adaptive control algorithms can automate low-level control tasks, enabling stable and consistent closed-loop dynamic behavior when the parameters of open-loop plant dynamics are uncertain. The idea of the shared control architecture introduced in this thesis is to allow human operators to focus on higher-level perception and decision-making tasks where their cognitive capabilities can be leveraged, while using adaptive autopilots for command tracking and regulation tasks. The autonomous control algorithms presented in this thesis build on two recent advances in adaptive control theory, namely the use of closed-loop reference models for improved transient performance, and computationally efficient control designs for output-feedback systems having relative degree two or greater.

In Chapter 3, a shared control architecture between on-board human pilots and adaptive controllers with full state information was presented. In Chapter 4, the shared control architecture was developed for remote human operators and adaptive controllers having just partial state information available for feedback control. In these two settings, the human operator collaborates with the autopilot in the detection and diagnosis of the anomaly and delegates corrective actions to an adaptive

flight control system. The targeted role of the human operator is motivated by the limitations that come with manual control of unfamiliar dynamical systems, as well as the cognitive and perceptive capabilities unique to human operators. Under our shared control framework, the human operator and adaptive autopilot designs form a shared response to dynamical anomalies.

The shared controllers defined in Chapters 3 and 4 are applied to several scenarios relevant to flight control through numerical simulations. The shared controller with on-board human pilots is demonstrated in the context of the control of roll dynamics of an aircraft in the presence of two different kinds of anomalies. In both cases, the pilot's task is to perceive if there is a change in the order of the vehicle dynamics, and convey this change to the adaptive autopilot. The resulting shared control action was shown to lead to satisfactory performance through detailed simulation studies. The shared control architecture using remote human operators and output feedback is demonstrated in simulations of the control of longitudinal dynamics of an unmanned high altitude, long endurance aircraft. It is shown how an anomaly response using the shared controller is able to avert structural failure following an anomaly which abruptly changes actuator dynamics, and restore nominal performance.

There are several directions in which this work can be extended. One area to explore is in the development of anomaly detection and diagnosis tools to aid the human operator, based on models of how humans perceive and diagnose anomalies. Demonstrating this work on hardware platforms with a human in/on the loop is another area for future work which would provide valuable insights and help to bring this work to a higher level of maturity. In summary, designing control architectures which are able to leverage the benefits of both humans and model-based algorithmic controllers may allow for both safer and more performant systems compared to what is achievable using humans or autonomous controllers alone, and this thesis has demonstrated one of many possible realizations of such a control design philosophy.

## Appendix A

### Numerical Simulation Parameters

Parameter	Value
$Q_{\text{LQR}}$	$\text{diag}(0.001, 2.0, 0.001, 2.0, 200, 50, 0.001, 0.001, 10.0, 0.00025)$
$R_{\text{LQR}}$	$50I_2$
$\alpha_0$	1.0
$\alpha_1$	0.5
$\epsilon$	20
$\Gamma_m$	$400I_3$
$\Gamma_\Lambda$	$\text{diag}(2000I_2, 0.2I_{14})$

Table A.1: Parameters used in the *nominal* adaptive controller for numerical HALE VFA simulations

Parameter	Value
$Q_{\text{LQR}}$	$\text{diag}(0.001, 2.0, 0.001, 2.0, \dots 200, 50, 0.001, 0.001, 0.0001, 0.0001, 0.5, 0.00005)$
$R_{\text{LQR}}$	$50I_2$
$\alpha_0$	2.0
$\alpha_1$	$\sqrt{2.0}$
$\alpha_2$	1.0
$\epsilon$	20
$\Gamma_\Theta$	$\text{diag}(2000I_2, 0.2I_{14})$
$\Gamma_\Psi$	$\text{diag}(1000I_6, 5000I_2)$
$\mu$	0.02

Table A.2: Parameters used in the *recovery* adaptive controller for numerical HALE VFA simulations

# Bibliography

- [1] Saurabh Amin, Alvaro A Cárdenas, and S Shankar Sastry. Safe and secure networked control systems under denial-of-service attacks. In *International Workshop on Hybrid Systems: Computation and Control*, pages 31–45. Springer, 2009.
- [2] Christine M Belcastro, John Foster, Richard L Newman, Loren Groff, Dennis A Crider, and David H Klyde. Preliminary analysis of aircraft loss of control accidents: Worst case precursor combinations and temporal sequencing. In *AIAA Guidance, Navigation, and Control Conference*, pages 10.2514/6.2014–0612, 2014.
- [3] Christine M Belcastro, John V Foster, Richard L Newman, Loren Groff, Dennis A Crider, and David H Klyde. Aircraft loss of control: Problem analysis for the development and validation of technology solutions. In *AIAA Guidance, Navigation, and Control Conference*, 2016.
- [4] Mica R Endsley. Toward a theory of situation awareness in dynamic systems. *Human Factors: The Journal of the Human Factors and Ergonomics Society*, 37(1):32–64, 1995.
- [5] Mica R Endsley. Automation and situation awareness. In Raja Parasuraman and Mustapha Mouloua, editors, *Automation and Human Performance: Theory and Applications*, pages 163–181. Lawrence Erlbaum, 1996.
- [6] Amir B Farjadian, Anuradha M Annaswamy, and David Woods. Bumpless reengagement using shared control between human pilot and adaptive autopilot. In *IFAC World Congress*, pages 5343–5348. IFAC, 2017.
- [7] Travis E Gibson, Anuradha M Annaswamy, and Eugene Lavretsky. Modeling for control of very flexible aircraft. In *AIAA Guidance, Navigation, and Control Conference*, pages 10.2514/6.2011–6202, 2011.
- [8] Travis E Gibson, Anuradha M Annaswamy, and Eugene Lavretsky. On adaptive control with closed-loop reference models: Transients, oscillations, and peaking. *IEEE Access*, 1:703–717, 2013.
- [9] Robert K Heffley and Wayne F Jewell. Aircraft handling qualities data. Technical Report NASA-CR-2144, Systems Technology, Inc., Hawthorne, California, 1972.

- [10] Ronald A Hess. Unified theory for aircraft handling qualities and adverse aircraft-pilot coupling. *Journal of Guidance, Control, and Dynamics*, 20(6):1141–1148, 1997.
- [11] Ronald A Hess. Modeling pilot control behavior with sudden changes in vehicle dynamics. *Journal of Aircraft*, 46(5):1584–1592, 2009.
- [12] Ronald A Hess. Modeling the pilot detection of time-varying aircraft dynamics. *Journal of Aircraft*, 49(6):2100–2104, 2012.
- [13] Ronald A Hess. Modeling human pilot adaptation to flight control anomalies and changing task demands. *Journal of Guidance, Control, and Dynamics*, 38(6):655–666, 2015.
- [14] Andrew J Kerns, Daniel P Shepard, Jahshan A Bhatti, and Todd E Humphreys. Unmanned aircraft capture and control via GPS spoofing. *Journal of Field Robotics*, 31(4):617–636, 2014.
- [15] Alan Kim, Brandon Wampler, James Goppert, Inseok Hwang, and Hal Aldridge. Cyber attack vulnerabilities analysis for unmanned aerial vehicles. In *Infotech@Aerospace 2012*. American Institute of Aeronautics and Astronautics, 2012.
- [16] Cheolhyeon Kwon, Weiyi Liu, and Inseok Hwang. Analysis and design of stealthy cyber attacks on unmanned aerial systems. *Journal of Aerospace Information Systems*, 11(8):525–539, 2014.
- [17] Thanh Mung Lam, Harmen Wigert Boschloo, Max Mulder, and Marinus M Van Paassen. Artificial force field for haptic feedback in uav teleoperation. *IEEE Transactions on Systems, Man, and Cybernetics-Part A: Systems and Humans*, 39(6):1316–1330, 2009.
- [18] Thanh Mung Lam, Max Mulder, and Marinus M Van Paassen. Haptic feedback in uninhabited aerial vehicle teleoperation with time delay. *Journal of guidance, control, and dynamics*, 31(6):1728–1739, 2008.
- [19] Eugene Lavretsky, Travis E Gibson, and Anuradha M Annaswamy. Projection operator in adaptive systems, 2012.
- [20] Eugene Lavretsky and Kevin A Wise. *Robust and Adaptive Control with Aerospace Applications*. Springer, 2013.
- [21] Charles C Macadam. Understanding and modeling the human driver. *Vehicle System Dynamics*, 40(1-3):101–134, 2003.
- [22] Jason S McCarley and Christopher D Wickens. Human factors concerns in UAV flight. 2004.

- [23] Duane T McRuer and Henry R Jex. A review of quasi-linear pilot models. *IEEE Transactions on Human Factors in Electronics*, (3):231–249, 1967.
- [24] Kumpati S Narendra and Anuradha M Annaswamy. *Stable Adaptive Systems*. Dover Publications, 2005.
- [25] Nick Oliver, Thomas Calvard, and Kristina Potočnik. Cognition, technology, and organizational limits: Lessons from the Air France 447 disaster. *Organization Science*, 2017.
- [26] Raja Parasuraman, Thomas B Sheridan, and Christopher D Wickens. A model for types and levels of human interaction with automation. *IEEE Transactions on Systems, Man, and Cybernetics-Part A: Systems and Humans*, 30(3):286–297, 2000.
- [27] Anil V Phatak and George A Bekey. Model of the adaptive behavior of the human operator in response to a sudden change in the control situation. *IEEE Transactions on Man-Machine Systems*, 10(3):72–80, 1969.
- [28] Jean-Baptiste Pomet and Laurent Praly. Adaptive nonlinear regulation: Estimation from the Lyapunov equation. *IEEE Transactions on Automatic Control*, 37(6):729–740, 1992.
- [29] Zheng Qu. *Adaptive Output-Feedback Control and Applications to Very Flexible Aircraft*. PhD thesis, Massachusetts Institute of Technology, 2016.
- [30] Zheng Qu, Anuradha M Annaswamy, and Eugene Lavretsky. Adaptive output-feedback control for relative degree two systems based on closed-loop reference models. In *IEEE Conference on Decision and Control (CDC)*, pages 7598–7603. IEEE, 2015.
- [31] Zheng Qu, Anuradha M Annaswamy, and Eugene Lavretsky. Adaptive output-feedback control for a class of multi-input-multi-output plants with applications to very flexible aircraft. In *American Control Conference (ACC), 2016*, pages 1613–1618. IEEE, 2016.
- [32] Thomas B Sheridan. Toward a general model of supervisory control. In *Monitoring Behavior and Supervisory Control*, pages 271–281. Springer, 1976.
- [33] Thomas B Sheridan. Adaptive automation, level of automation, allocation authority, supervisory control, and adaptive control: Distinctions and modes of adaptation. *IEEE Transactions on Systems, Man, and Cybernetics-Part A: Systems and Humans*, 41(4):662–667, 2011.
- [34] Thomas B Sheridan and Raja Parasuraman. Human versus automation in responding to failures: An expected-value analysis. *Human Factors*, 42(3):403–407, 2000.

- [35] Brian L Stevens, Frank L Lewis, and Eric N Johnson. *Aircraft Control and Simulation: Dynamics, Controls Design, and Autonomous Systems*. John Wiley & Sons, 2015.
- [36] Hong Z Tan, Mandayam A Srinivasan, Brian Eberman, and Belinda Cheng. Human factors for the design of force-reflecting haptic interfaces. In *Dynamic Systems and Control*, volume 55, pages 353–359, 1994.
- [37] Anthony P Tvaryanas and William T Thompson. Recurrent error pathways in HFACS data: Analysis of 95 mishaps with remotely piloted aircraft. *Aviation, Space, and Environmental Medicine*, 79(5):525–532, 2008.
- [38] Gi-Hun Yang, Ki-Uk Kyung, Mandayam A Srinivasan, and Dong-Soo Kwon. Development of quantitative tactile display device to provide both pin-array-type tactile feedback and thermal feedback. In *Proceedings of the Second World Haptics Conference*, pages 578–579. IEEE, 2007.
- [39] Peter MT Zaal. Manual control adaptation to changing vehicle dynamics in roll-pitch control tasks. *Journal of Guidance, Control, and Dynamics*, pages 1046–1058, 2016.
- [40] Peter MT Zaal and Barbara T Sweet. Estimation of time-varying pilot model parameters. In *AIAA Modeling and Simulation Technologies Conference*, 2011.
- [41] Youmin Zhang and Jin Jiang. Bibliographical review on reconfigurable fault-tolerant control systems. *Annual Reviews in Control*, 32(2):229–252, 2008.